

CLOSED LOOP VIRTUAL REALITY FOR THE TREATMENT OF PHOBIAS

Bachelor Thesis

Systems Neuroscience & Neurotechnology Unit
Saarland University of Applied Sciences
Faculty of Engineering

Submitted by : Dominik Limbach

Matriculation Number : 3662306

Course of Study : Biomedical Engineering (Bachelor)

First Supervisor : Prof. Dr. Dr. Daniel J. Strauss

Second Supervisor : Dr. Lars Haab

Saarbrücken, March 26, 2018

Copyright © 2018 Dominik Limbach, some rights reserved.

Permission is hereby granted, free of charge, to anyone obtaining a copy of this material, to freely copy and/or redistribute unchanged copies of this material according to the conditions of the Creative Commons Attribution-NonCommercial-NoDerivatives License 4.0 International. Any form of commercial use of this material - excerpt use in particular - requires the prior written consent of the author.



<http://creativecommons.org/licenses/by-nc-nd/4.0/>

Declaration

I hereby declare that I have authored this work independently, that I have not used other than the declared sources and resources, and that I have explicitly marked all material which has been quoted either literally or by content from the used sources. This work has neither been submitted to any audit institution nor been published in its current form.

Saarbrücken, March 26, 2018

Dominik Limbach

Abstract

Virtual reality is a high-end user-computer interface that combines real-time computer graphics, body-tracking devices and high-resolution visual displays to create a computer-generated virtual environment. Its implementation into the treatment of anxiety disorders, such as phobias, has been studied extensively over the past decades.

The combination of exposure therapy and virtual reality environments, called virtual reality exposure therapy, provides for an efficient alternative to traditional in-vivo exposure. In an attempt to improve upon virtual reality systems that have been used in the past, we created a closed loop virtual reality system that features an adaptable virtual reality environment and real-time measures of sympathetic fear responses.

We have designed our virtual reality environment specifically for the treatment of acrophobia for its intended use in a psychological study on the matter.

In an preceding experiment, 11 subjects were exposed to a visual height challenge inside the virtual reality environment. During the exposure, the skin response level as well as heart-rate variation of the subjects were measured and displayed to the user, controlling the virtual reality. By presenting the extracted features, we relay crucial information about the patient's current mental state and provide a support tool for the therapist's decision making and therefore a possible improvement to the quality of virtual exposure therapy.

The objective of the present thesis, other than designing the virtual reality environment, was to provide for signal processing and feature extraction to assist in the creation of a classification tool.

Zusammenfassung

translation of abstract

Acknowledgments

give thanks to

- Prof. Dr.Dr. D.J.Strauss
- Dr. L. Haab
- everyone else contributed

Firstly, I want to give thanks to Prof. Dr.Dr. D.J.Strauss and every member of the Systems Neuroscience and Neurotechnology Unit for providing a kind and supportive work environment. Further I would to thank Dr. Lars Haab

Contents

Declaration	3
Abstract	1
Zusammenfassung	2
Acknowledgments	3
1 Introduction	6
1.1 Motivation	6
1.2 Theoretical Background	6
1.2.1 Fear and Phobia	7
1.2.2 Exposure Therapy	10
1.2.3 Electrodermal Activity	11
1.2.4 Electrocardiogram	24
1.3 General	30
1.3.1 Related Work	30
1.3.2 Problem Analysis and Goals	32
2 Materials and Methods	34
2.1 Materials	34
2.1.1 System Components	34
2.1.2 Hardware	34
2.1.3 Software	37
2.1.4 Virtual Environment	38
2.1.5 Virtual Reality Setup	41
2.2 Methods	43
2.2.1 Participants	43
2.2.2 Procedure	43
2.2.3 Virtual Reality Control	45
2.2.4 Data Acquisition	47
2.2.5 Data Processing	48
2.2.6 Feature Extraction	52
3 Results	58
3.1 Electrodermal Activity	58
3.2 Electrocardiogram	61

3.3 Statistical Results	63
4 Discussion	65
5 Conclusions	66
A Tables and Measurement Results	67
List of Figures	68
List of Tables	70
Bibliography	71

1 Introduction

1.1 Motivation

Anxiety disorders, such as acrophobia, can be a huge interference in many aspects of daily life. Although the severity of the phobia may vary from one individual to another, affected individuals are often experiencing a slowly progressing self-limitation fueled by their fear, resulting in a steadily declining quality of life. At this point a well executed therapy is the only chance for the phobic to overcome his fear and return to a normal way of life. Although, in-vivo exposure has proven to be an efficient treatment, the majority of phobics hesitate to accept therapy. This comes as no surprise, considering a traditional exposure therapy involves a direct confrontation with the fear stimulus. In addition, therapy is often held in an unfamiliar and dangerous environment, involving a genuine risk of injury. A fact which is intimidating for most people, but especially for patients with fear of heights. A virtual reality exposure on the other hand offers the possibility to treat patients in a controlled environment, eliminating the risk of injury and making it more likely to be accepted by the patient. Additionally, VR therapy systems become equally appealing for therapists considering technical advances have lowered the initial costs substantially and the amount of time and effort that can be saved by VR treatment. Despite all this however, many physicians are still resilient, when it comes to VR therapy. In cooperation with the Psychiatry Department of the University Hospital Homburg we want to develop a VR treatment system for acrophobia that fits the needs of the therapist and provides for a simple and efficient solution to conduct quality therapy.

1.2 Theoretical Background

In this chapter, we will give a brief introduction to the field of anxiety disorders, especially specific phobias and the associated therapy concept, which is exposure therapy. The first part will contain fundamentals on phobias, exposure therapy and the concept of fear. Furthermore we will elaborate on the psychophysiological influences of stress and anxiety on certain parts of the human body and functions as well as methods of determination in physiological measurement. The second part will recapitulate recent approaches on virtual reality exposure therapy and analyze existing problems.

1.2.1 Fear and Phobia

Why are we afraid? Over the course of history there has been one distinct answer to this question - survival. If we could not fear we would not be able to survive. Missing the ability to recognize and react appropriately to dangerous situations would spell doom on us as a species. From the beginning of human evolution, those that feared the right things survived and therefore were able to pass on their genes. Doing so, the trait of fear and the response to said fear were also passed on, ensuring the future survival of the race. In today's times humans no longer have to survive in the wild. However, fear is still rooted deep in our brains, serving the same purpose. Therefore "the decision to not take that shortcut through the deserted alley at midnight is based on a rational fear that promotes survival" [1]. But what actually is fear? In a review of Öhman's work (2000) Fink describes fear as an "activated, aversive emotional state that serves to motivate attempts to cope with events that provide threats to the survival or well-being of organisms" [2]. These coping attempts involve defensive behaviors such as immobility, escape and attack, of which the latter two are typically described as the flight or fight response. Although not as obvious, there are far more aspects to a fear response than the observable behavior, especially physiological responses. However, how we react to a certain fear stimulus heavily depends on the immediate situation. Because fear is strongly related to the activation of the autonomic nervous system, our response is therefore depending on the direction of this activation. For example if we face a non imminent threat, which appears stationary, we generally tend to respond calm and collected, redirecting our attention towards the potential threat stimulus. Whereas, in a situation with an imminent or approaching danger, the sympathetic branch of the autonomic nervous system is activated, which is accompanied by heart rate acceleration, blood pressure increase and release of catecholamines from the adrenal medulla. This allows for physical peak performance and we respond with flight or fight.

Fear Measures

Considering the importance of fear to the human evolution it comes as no surprise that fear and, more specifically, the assessment of fear have been frequent subjects to a number of studies. There are many different ways to measure fear, most of which are derived from the specific components of fear. Other than interviewing the subject and assessing their subjective fear rating there are measures that directly derive fear indices from effectors innervated by the autonomic nervous system. Several of these measures, such as heart rate deceleration and skin conductance response, are primarily associated with the increased attentiveness in the initial states of fear. Measures, such as heart rate and blood pressure on the other hand, reflect the sympathetic mobilization [2]. It is to mention that these measures are not necessarily intercorrelated, even when assessing the effects of the same fear stimulus. This is because a fear response is rather a combination of

different and partially independent response components, which are sensitive to multiple modulating parameters.

Fear stimuli

In general a fear stimulus can be described as an event, situation or object that provides a threat to the integrity of a person, either in a physical or in a psychological sense. Fear stimuli can be divided into physical, animal and social stimuli [2]. In the interest of the present thesis we will focus on stimuli that originate from the physical environment, especially those that have provided a recurrent threat throughout the human evolution and therefore prove highly effective in eliciting fear and associated flight attempts. Fitting this pattern are physical stimuli such as wide open spaces, darkness and heights.

The intensity of a stimulus is a key component regarding the strength of the elicited fear reaction. It is modulated by a number of factors such as distance to the stimulus, stimulus predictability and movement of the stimulus. For example a close or approaching stimulus, which was not expected would elicit the highest amount of fear. In addition to the evolutionary stimuli there are, so-called, learned stimuli, which are former neutral stimuli that acquired their fear-eliciting power through learning. Fear learning typically occurs when the neutral stimulus and a natural fear triggering stimulus are presented at the same time and the fear may be transferred.

The Neurophysiology of Fear

As mentioned above fear is a protection mechanism that is rooted in our brain. The neural network that controls the fear response as well as the learning of fear was found to be built around the amygdala. The amygdala was identified as a part of the limbic system, which is associated with emotion and can be described as a collection of interconnected nuclei in the anterior temporal lobe [2]. Its primary function is the evaluation of threats by filtering sensory information from the cortex and the subcortical structures such as the thalamus. These two routes of information delivery have been described as the high and the low route. The low route is a monosynaptic connection between the thalamus and the amygdala. Therefore the information conveyed by this route reaches the amygdala faster than the information conveyed by the polysynaptic high route, allowing for a defense response to start even before the threat stimulus is confirmed by the full cortical analysis. Thus, only the low route is considered necessary for fear elicitation and fear learning. Once the threats have been evaluated by the lateral and basolateral nuclei of the amygdala the information is passed on to the central nucleus from where the efferent aspects of the fear response are controlled. Through neural pathways, leading to the lateral hypothalamus, sympathetically controlled responses, such as heart-rate acceleration and skin conductance responses, and parasympathetically

dominated responses, such as heart-rate deceleration, are then activated and therefore complete the fear response.

There are however instances where fear exceeds its purpose and becomes pathological. An intense, involuntary and irrational fear of a specific stimulus, that causes a maladaptive avoidance is called a phobia [2]. According to the three kinds of stimuli phobias are also classified into three categories, of which we will focus on the specific phobias.

Specific Phobia

A specific phobia is a marked and persistent fear elicited by a specific object or situation. Upon exposure to, or in anticipation of the phobic stimulus, the individuals, afflicted with the phobia, experience almost invariably an excessive or unreasonable fear. Thus, the phobic stimulus is generally avoided and therefore a behavioral pattern is formed. This avoidance behavior can eventually lead to a severe interference of the individual's daily routine, occupational functioning and social life. According to the focus of the fear, specific phobias are categorized in subtypes, such as animal type or natural environment type. Some types of phobias may also involve concerns about loss of control, panic and other fear related symptoms, such as vertigo, which is experienced by many people suffering from a fear of heights. As mentioned earlier the level of fear, elicited by the phobic stimulus, usually depends on certain factors such as proximity or movement. There are however cases when there is a discrepancy between the expected intensity of the fear reaction and the actual response in regard to the strength of the phobic stimulus. For example, the amount of fear, experienced by a height fearing individual crossing a bridge, can vary between different occasions. According to the Diagnostic and Statistical Manual of Mental Disorders, Fourth Edition, a 1-year prevalence of 9% has been found in community samples, with lifetime rates ranging from 10% to 11.3%, for specific phobias [3]. Depending on the subtype the course and the mean age of onset varies. Phobias of the natural environment type primarily begin in childhood, although a second peak in early adulthood has been observed for fear of heights particularly. "Predisposing factors to the onset of specific phobias include traumatic events, unexpected panic attacks in the to-be-feared situation, observation of others undergoing trauma or demonstrating fearfulness, and informational transmission" [3]. Phobias that persist into adulthood often remain permanent and require therapy in order to be cured. Before enlarging upon the treatment of specific phobias we will have a brief look at acrophobia, which will be in the center of the present thesis.

Acrophobia

Acrophobia, which is an extreme or irrational fear of heights, is considered a specific phobia of the natural environment type [3]. Afflicted individuals typically display avoidance towards a variety of height-related situations, including scenarios such as stairs, bridges, windows in high buildings and even elevators and flying. Considering the number of stimulating situations, it comes as no surprise that acrophobia heavily impairs afflicted individuals in their daily life. In addition acrophobia has shown to be one of the most common phobias in the general population. Kapfhammer et al. (2015) found that the lifetime prevalence of acrophobia, in a sample of 2012 individuals aged 14 and above, was 6.4% (8.4% women, 4.1% men). Further, a lifetime prevalence of 28.5% for visual height intolerance was reported, of which 22.5% have experienced panic attacks and in 6.4% developed into acrophobia [4].

1.2.2 Exposure Therapy

Anxiety disorders occur when neutral stimuli become threatening and therefore cause irrational fear and avoidance, in the afflicted individuals. Exposure therapy is a treatment procedure, which is designed to reduce pathological fear and avoidance of the feared object or situation by intentionally confronting the patient with the feared stimulus in an otherwise safe environment. Foa and Kozak (1986) suggested this effect to be achieved through emotional processing. Emotional processing can be described as a process by which accurate information is implemented into the fear structure and alters the pathological elements in the structure. However, more recent studies suggest that exposure therapy rather creates competing structures that do not include pathological associations among stimulus, response and meaning representation instead of altering existing ones [5]. Further, O'Donohue and Fisher (2012) described two major conditions that are necessary for emotional processing to be successful and fear reduction to occur. "First, the fear structure must be activated for it to be available for modification. Second, new information that is incompatible with the pathological elements of the fear structure must be available and incorporated into the pathological memory structure (or form a new nonpathological competing structure)" [5]. Exposure therapy efficiently satisfies both conditions as approaching the feared object or situation is likely to trigger the fear structure and at the same time providing corrective information through the absence of dreaded consequences, allowing for a successful learning process.

1.2.3 Electrodermal Activity

Electrodermal activity (EDA) is a collective term for all electrical phenomena in the skin, which was first introduced by Johnson and Lubin (1966). This includes active and passive electrical properties, caused by skin functions and skin structure as well as the appendages of the skin [6]. The skin appendages are structures formed by skin-derived cells such as hair, nails, sebaceous glands and sweat glands. EDA is one of the most commonly used response systems in psychophysiological research. This is due to its relative ease of measurement and its sensitivity to psychophysiological states and processes. The following section will provide a brief overview of EDA, ranging from physical and psychological context to recording and quantification methods.

Anatomical basis

This section will elaborate on the anatomical aspects of the human skin and will cover all the parts and appendages, that are needed to understand the principles of EDA. The skin or cutis is the biggest organ of the human body and inherits many different functions, which are essential for survival. It primarily acts as a selective barrier, preventing the entry of foreign matter and enables the passage of materials from the bloodstream to the exterior of the body. Other than protection, it is involved in thermoregulation, cutaneous circulation and immunologic protection. The anatomical structure of the skin is similar in most regions of the body. Although, specialized regions of skin, such as the palms and soles may be resembling in structure, they possess modified characteristics [7].

The human skin is composed of two clearly distinguishable layers, the epidermis that serves as a protective barrier and the dermis that provides nutrition. The cutaneous structures are vertically arranged and located on top of the subcutaneous tissue. Figure 1.1 shows a representation of each of the layers and their general spatial configuration among themselves. However, the zonal layering is not distinct in every skin region (e.g., the stratum lucidum is only clearly recognizable on the palmar and plantar skin areas)[6].

The epidermis, on its own, can be divided into five different layers and lies on the surface of the skin. It consists of epithelial tissue, which is built in the lowest layer, the stratum germinativum. The main part of the produced cells are keratinocytes, which are able to store keratin and therefore become horny over time. The keratinocytes migrate to the surface of the skin, causing the epidermis to become more horny when approaching the surface. The outer layer is called the stratum corneum, originating from the fully keratinized state of its cells. On their way to the surface the keratinocytes undergo a number of specific changes in form and areal distribution, which in part are used to define the different epidermal layers. Also the cells become less tightly packed, compared

		Stratum corneum	upper zone middle zone lower zone	
	Epidermis	Stratum lucidum Stratum granulosum (granular layer)		Stratum intermedium
Cutis (skin)		Stratum spinosum (prickle cell layer) Stratum germinativum (basal layer)		Stratum Malpighii
	Dermis (cutis vera = true skin)	Stratum papillare (papillary layer) Stratum reticulare (reticular layer)		
	Subcutis (hypodermis)			

Figure 1.1: The Layers of the skin.

to the deeper layers, causing the epidermis to become dryer towards the surface. A fact that greatly influences the electrical properties of the epidermis and therefore the electrodermal activity. The stratum corneum is especially thick in the palmar and plantar regions of the body. Reaching a thickness of approximately 1 mm , it is almost 20 times thicker than its overall average of $50\text{ }\mu\text{m}$.

The dermis, which is also referred to as the corium, lies directly beneath the epidermis. Although it is much thicker than the epidermis it is only composed of two different dermal layers, the stratum papillare and the stratum reticulare, which are distinguishable by their density and the arrangement of their collagen fibers. The epidermal dermal junction, which is the transition area between the epidermis and dermis, resembles interlocking hands and is formed by a basal-membrane zone [6]. The dermal layer, closest to the epidermis is called the papillary stratum. Other than the capillary net of arterial and venous blood vessels, it contains receptor organs as well as melanocytes and free collagen cells. The second dermal layer, which lies on top of the subcutaneous tissue, is called the reticular stratum. It wears this name because of its texture. Formed of strong collagenous fibers, reticular stratum is highly resistant to rupture, granting the dermis its leathery impression.

The subcutis, or hypodermis, is located beneath the dermis and is composed of loose connective tissue. It serves as a connection between the skin and the connective tissue of the muscles, allowing for good horizontal mobility of the skin. The subcutis also serves as a thermal and mechanical insulation layer, due to its ability to store fat. In addition to this it, contains nerves and vessels, which supply the skin with nutrition and information, as well as the hair follicles and secretory part of the glands.

The left side of figure 1.2 shows an example for a typical profile of glabrous (hairless)

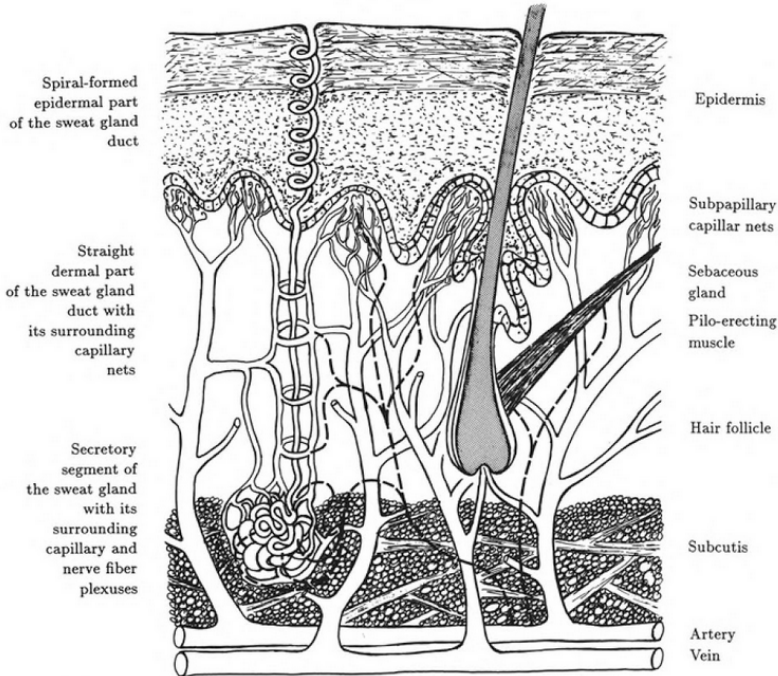


Figure 1.2: A artificial cross-section of the skin, combining a sweat gland in ridged skin (left) and a hair together with a sebaceous gland in polygonal skin (right).

skin. This specific form of skin differs in its horizontal structure. During early embryonal development specific patterns are formed by ridge formation. Ridged skin can be found on the palms of the hands and the soles of the feet. Areas, both of which, are frequently mechanically stressed and also have been found to have the highest densities of sweat glands, with an average of 233 sweat glands per cm^2 on the hands and 620 glands per cm^2 in adult's skin [6]. Sweat gland are considered to be exocrine glands, which is due to the fact that they secrete directly onto the surface of the skin. There are two types of human sweat glands, eccrine and apocrine, the majority being of the first type. The secretions of eccrine glands only contain negligible amounts of cytoplasm from the glandular cells. As there are no apocrine sweat glands located on the palmar skin, which is the most common location for EDA measurement, this section will only focus on eccrine sweat glands. The main purpose of eccrine sweat glands is to regulate the body temperature. With the exception of the palmar and plantar glands, which are thought to rather take part in grasping behavior [8]. Further all eccrine sweat glands are believed to be more responsive to psychologically significant stimuli and therefore to be involved in emotional sweating. Emotional sweating is primarily observable in areas with a high density of eccrine sweat glands, such as hands and feet. Therefore, making these region particularly interesting for EDA measurement, concerning the effect of psychophysiological stimuli. Before elaborating on the connection between electrodermal activity and sweat gland activity, it is useful to consider the anatomy of the glands first.

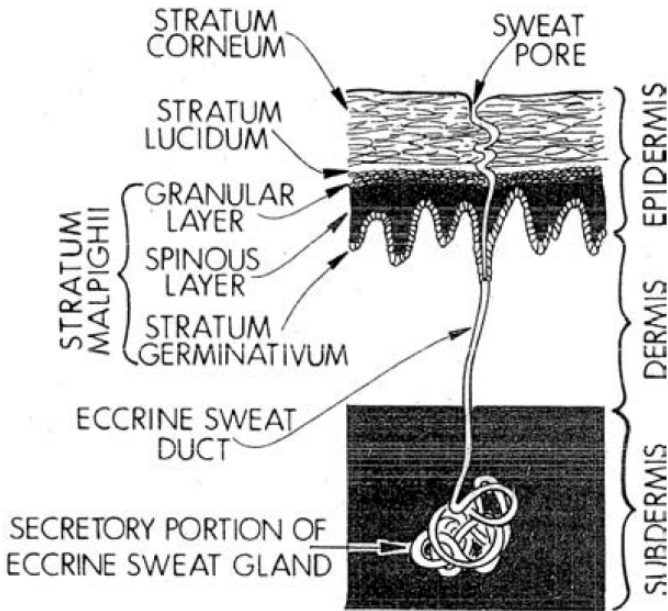


Figure 1.3: Anatomy of the eccrine sweat gland in various layers of glabrous skin.(Adapted from Hassett, 1978)

Figure 1.3 shows the anatomy of an eccrine sweat gland in glabrous skin. It consists of the secretory portion, the coiled compact body of the gland, and the sweat duct. The sweat duct, which is the excretory portion of the gland, is a long tube reaching all the way to the stratum corneum, forming a small pore on the surface of the skin. It passes through the dermis in a relatively straight line but ends up spiraling through the epidermis [8]. Imagining sweat glands as a set of variable resistors wired in parallel, helps to understand their influence on electrodermal activity. As sweat rises in the ducts their electrical resistance is constantly reduced, resulting in noticeable changes in electrodermal activity. The amount of sweat and the number of glands that are currently active, and therefore the electrodermal activity depends on the degree of activation of the sympathetic division of the autonomic nervous system.

Physiological basis

According to the previous section, focusing on the anatomical aspects, this section will outline only the physiological mechanisms required to understand electrodermal mechanisms. The autonomic nervous system (ANS) is a complex systems of nerves that regulates involuntary and unconscious actions. The emphasis of this section will be its thermoregulatory aspects, which also involve the skin and sweat glands. There are a number of efferent vegetative fibers in the human skin, including sympathetic fibers, innervating the secretory segment of the eccrine sweat glands, and vasoconstrictive

effences for the blood vessels. Originating from the brain, the efferent sympathetic nerves descend in the anterolateral part of the spinal cord in close proximity to the pyramidal tract. They are switched over in the lateral horn and leave the spinal cord through its ventral root. Alongside motoric fibers, the preganglionic sympathetic fibers travel via the white communicating ramus to the sympathetic trunk. From this point the neuronal activity will be distributed to various levels of the sympathetic trunk, causing one preganglionic fiber to reach up to 16 postganglionic neurons. The postganglionic fibers exit the sympathetic trunk through the gray communicating ramus and from there spread into the periphery, eventually reaching the skin. Human sweat glands have predominantly sympathetic cholinergic innervation from sudomotor fibers originating in the sympathetic chain. The secretory part of the gland is surrounded by a dense plexus of sympathetic fibers. This allows for a wide distribution of ANS activity. The sudorissecretory fibers form a smooth bundle between the lateral pyramidal tract and the anterolateral tract. They end at the preganglionic sudorissecretory neurons and run right next to the other sympathetic fibers. Although the sympathetic system is represented in various locations of the brain, the hypothalamus is considered to be the controlling entity of all vegetative functions. This includes sweat secretion and vasomotor activity. However, the central innervation of sweat gland activity is not limited to the hypothalamus. There are several centers, which are located in different levels of the central nervous system and partly independent of one another. The cortex, the basal ganglia, diencephalic structures such as thalamus and hypothalamus, the limbic system and brain stem areas are considered possible origins of sympathetic activity [6].

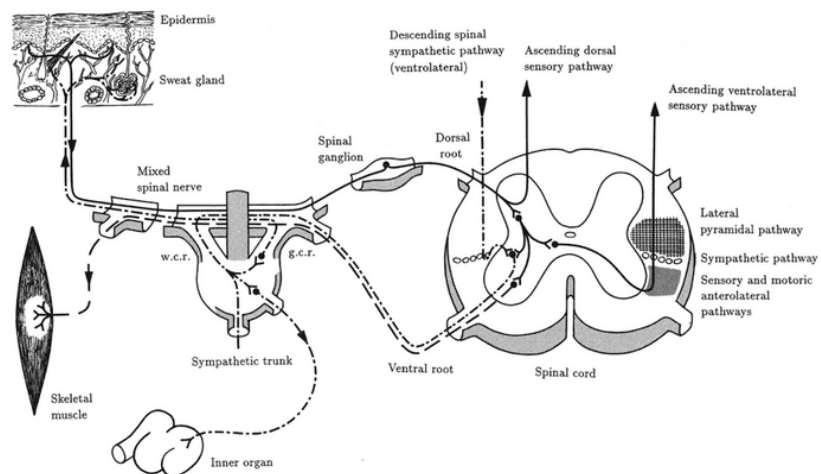


Figure 1.4: Skin afferents and efferents at spinal cord level and connections with ascending and descending pathways. —: motoric pathway, -.-: sympathetic efferents.

Physiology of Electrodermal Activity

Studies, measuring sympathetic action potentials in peripheral nerves while simultaneously recording EDA, have shown a high correlation between bursts of sympathetic nerve activity and the phasic skin conductance response [8]. Because there are many excitatory and inhibitory influences on the sympathetic system, located in various parts of the brain, there also are a variety of neural mechanisms and pathways involved into the central control of EDA. In a review on CNS elicitation of EDA, Boucsein (2013) concludes that there are two different origins above reticular level: a limbic-hypothalamic source, which is also thermoregulatory and emotionally influenced, and a premotor-basal ganglia source, eliciting electrodermal concomitants of the preparation of specific motor actions. In addition, Boucsein suggests a third reticular modulating system, mediating EDA changes appearing with variations of general arousal (see figure 1.5). Further, an inhibitory EDA system has been located in the bulbar level of the reticular formation.

However, there are also properties of the skin, influencing the EDA, which have to be considered, especially local physiological phenomena related to sweat gland activity. Considering the vertical structure of the skin, there is a significant difference in conductivity between the different layers. Both the dermis and the subcutis are tissues with strong blood supply and interstitial fluid. Therefore their electrical conductivity is much higher than the conductivity of the epidermal layer, which forms a diffusional as well as an electrical barrier. There has been some discussion concerning the exact localization of an epidermal diffusional barrier, which has been reviewed in detail by Fowles (1986)(see [6]). However, most of the findings suggest that the entire stratum corneum is forming the barrier, with the exception of its desquamating surface cells[6]. It is to mention that, under normal physiological conditions, the skin temperature is causing changes in permeability of the skin. Fowles (1986) pointed out that the permeability for water doubles with an increase in skin temperature of 7-8 °C within the range of 25-39 °C (see [6]). In spite of the diffusional barrier and without activity of the sweat glands, there is always a continuous transmission of water in the skin, directed from the dermis to the outside of the body. This causes the corneum to be always partially hydrated. However, there is a distinct relationship between the relative humidity of the air and the corneal hydration, caused by a dependency of corneal thickness on the relative humidity of the air. As mentioned above there are differences in conductivity in the different skin layers. The barrier, formed by the outer epidermal layers, is penetrated by the sweat gland ducts, which act as diffusional and electrical shunts. Other than these properties, concerning the resistance, living tissue has capacitative features which are related to the activity of its membranes. While tissue conductivity is mainly responsible for tonic EDA and, in small parts, contributes to phasic electrodermal phenomena with rather slow recovery, active membrane processes following a nerve impulse are prone to eliciting electrodermal responses with fast recovery [6].

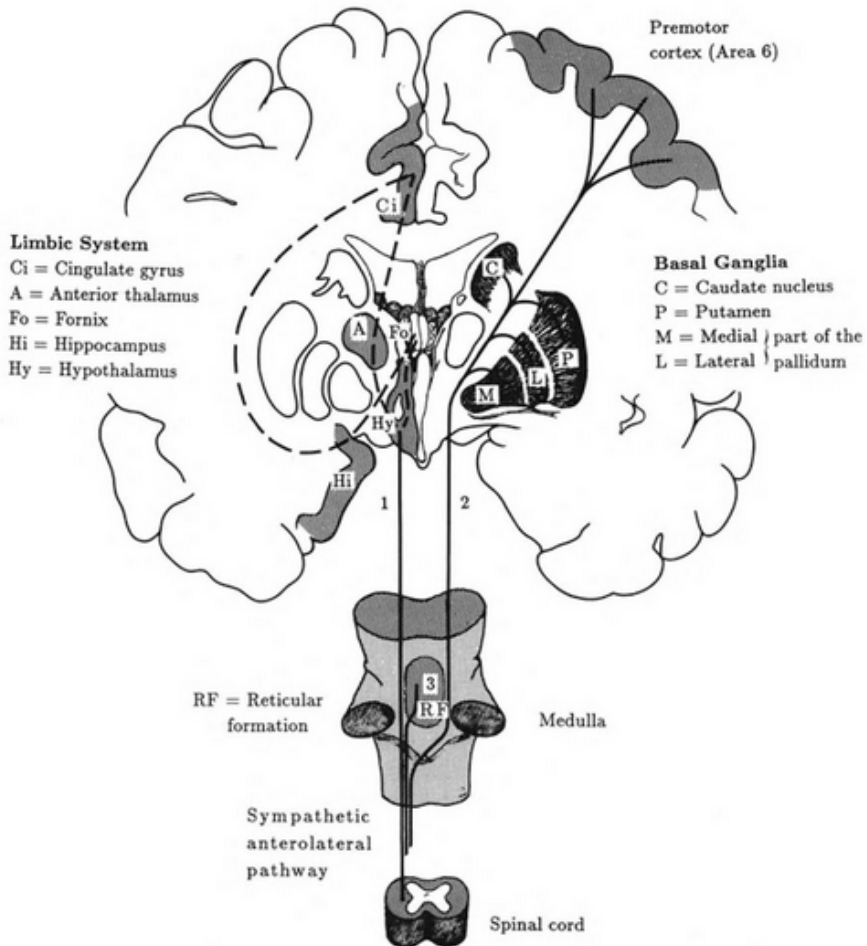


Figure 1.5: Central elicitation of EDA in humans. 1: Ipsilateral influences from the limbic system via hypothalamic thermoregulatory areas; 2: Contralateral influences from premotor cortical and basal ganglia areas; 3: Reticular influences. Dashed: Connections within the limbic system.

Principles of Electrodermal Measurement

There are three different methods of measuring EDA: the endosomatic method, which does not rely on the application of an external current, and two exosomatic methods, which apply either direct current or alternating current. For the past couple of decades the measurement of EDA as skin conductance, using a direct current, constant voltage methodology with silver-silver chloride (Ag/AgCl) electrodes and an electrolyte of sodium or potassium chloride has been the most prevalent method in EDA literature [9]. Thus, the present section will focus on this method. Typically, a small voltage (e.g., 0.5V) is applied to two electrodes, which are placed on the sound surface of the skin, and a small resistor (e.g., 200 to 1000 Ω) is connected in series with the skin. To avoid any electrocardiogram artifacts, the electrodes should be placed on the same body side.

Because the skin resistance exceeds the resistance of the resistor by far, its effect on the current flow inside the circuit can be neglected, when measuring the current flow. Hence, when applying Ohm's law, the current (I) flow between the electrodes, and therefore through the resistor, is equal to the voltage (U) divided by the Resistance of the skin (R_p).

$$I = U/R_p \quad (1.1)$$

Because the voltage has a constant value, the current changes in proportion to the reciprocal of the resistance, which is called conductance (G_p).

$$I \approx 1/R_p \quad (1.2)$$

Consequently, the conductance is proportional to the current flow through the skin.

$$I = U \cdot G_p \quad (1.3)$$

The unit of conductance is siemens (S), where $1 S = 1/1 \Omega$. According to the skin resistance usually being in the orders of $k\Omega$ or $M\Omega$, the conductance is very small and often measured in units of μS . Because the value of the series resistor (R_s) is constant, the voltage drop across R_s is proportional to the current flow I .

$$U = I \cdot R_s \quad (1.4)$$

Considering, the proportionality of I and G_p , as shown in 1.3 it becomes clear that changes in U can be monitored to provide precise index of variations in the skin conductance.

Techniques of Electrodermal Recording

This section will give a brief overview on possible requirements for electrodermal recording, such as special electrodes, electrode gels and recording devices.

Electrodes

Electrodes are a biomedical sensor system. Electrodermal recording typically relies on metal electrodes. However, metal being a generic term, as it is corroded at the surface of

the electrode. Different metals will cause different stages of corrosion. Therefore, when measuring EDA with a direct current ,it is of great importance to use two electrodes of the same material, eliminating eventual potential differences. In exosomatic recording, using a direct current, the electrode pair is connected to an external voltage. Thus, turning them into anode and cathode in an electric system, which are polarized by electrolysis. The standard electrodes, used in electrodermal recording, are sintered silver-silver chloride (Ag/AgCL) electrodes, which minimize both the polarization of the electrode and the bias potential between the electrodes. The most common form of EDA electrodes consist of a metal ring, which is embedded in a cylindrical plastic case. The space between metal and skin is filled with an electrode gel, which usually contains a chloride salt like NaCl. The concentrations of the electrode gel is chosen in the range of 0.050-0.075 molar to resemble the NaCl concentration in human sweat. Therefore, the concentration of the gel will remain stable when mixed with sweat. When using an electrolyte, it is recommended to fix the electrodes to the skin at least 5-10 minutes before starting the recording. This will eliminate an initial baseline drift in the EDA recording, caused by the electrolyte penetrating the stratum corneum and the sweat ducts. Further the electrode-skin impedance is greatly influenced by the size of the electrolyte-skin contact area and not the size of the electrode metal [9]. Therefore it is important to give special attention to the electrode fixation, guaranteeing a sufficient electrode-skin contact and a minimization of movement artifacts.

Recording Sites

Psychophysiological recordings rely on nonthermoregulatory electrodermal phenomena, which can be most reliably recorded from glabrous skin. Thus making the palms of the hands and the soles of the feet the preferred recording sites for EDA. There are three different ways to place the electrodes when recording EDA on the hand (see Figure 1.6).

Placement # 1 involves volar surfaces of medial phalanges, placement # 2 involves volar surfaces of distal phalanges, and placement # 3 involves thenar and hypothenar eminences of palms [8]. It is suggested to place electrodes on the palm of the nondominant hand, presuming it is not as likely to have as much horny skin. In addition, the placement method # 2 should be preferred over method # 1 because of the greater responsivity and the greater sweat gland activity of the distal phalanges, compared to the other placement sites [9].

If both hands are not available for recording, EDA can also be measured at the inner site of the foot , over the abductor hallucis muscle adjacent to the sole and in between the proximal phalanx of the big toe and a point directly beneath the ankle [9]. In case of exosomatic recording, there is usually no further pretreatment of the skin needed than washing the recording site with warm water.

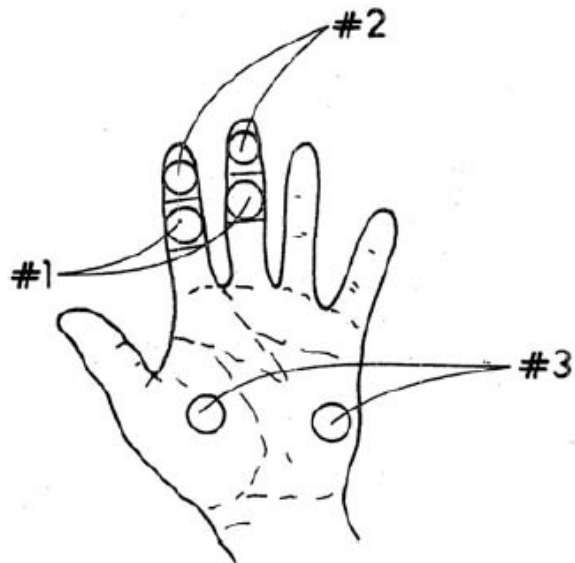


Figure 1.6: Three electrode placements for recording EDA.

Signal Evaluation

The EDA signal consists of two components, the slow, tonic skin conductance level (SCL) and the faster, phasic skin conductance response (SCR), which need to be addressed separately during the evaluation of the signal.

Phasic Electrodermal Measures

Electrodermal responses (EDRs) are short-lasting changes in EDA. They can be elicited by a distinct stimulus or occur without previous stimuli, therefore being called nonspecific EDRs (NS-EDRs). NS-EDRs are considered a tonic measure, meaning they are used to index EDA over a certain time period. In both cases the signal curve follows a certain pattern.

As shown in figure 1.7, there is a characteristic rise from the initial level to a peak, followed by a slower decline. In case of an elicited EDR the time that passes from the stimulus to the onset of the EDR is called latency (EDR lat.), which usually ranges from 1-4 seconds. As pointed out by Boucsein et al. (2012), latencies greater than 4 seconds may occur, but latencies under 1 second should be treated with caution because of system immanent temporal delays, such as time required for stimulus processing, autonomic nervous system nerve conduction to the sweat glands, and penetration of sweat through the ducts to the epidermis. Following the latency, there is an ascent time

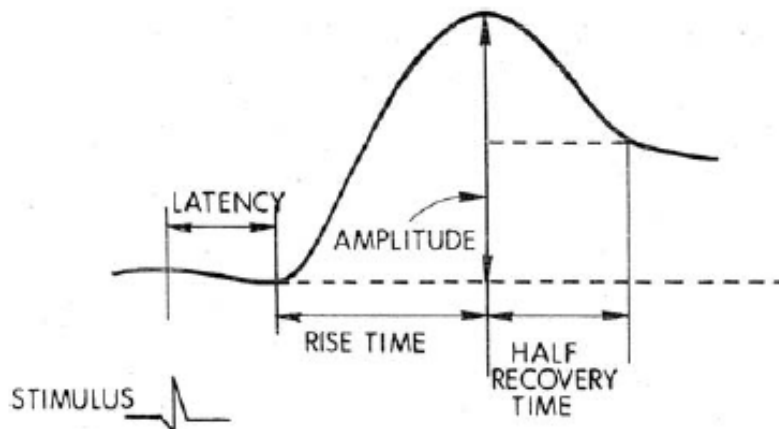


Figure 1.7: Graphical representation of principal EDA components.

from the initial level to the peak, which typically varies between 0.5 and 5 seconds [9]. The peak amplitude (EDR amp.) is reached. To determine the exact value of EDR amp., it is necessary to locate the onset point. Usually, this is done by stepping back along the SCR curve and finding the point of maximum curvature. At times it can be important to determine whether a response has occurred. The occurrence is therefore defined in terms of a minimum amplitude, that has to be reached in order for the event to be counted as a response. This is especially true for NS-EDRs. In the past the threshold value for the minimum amplitude was commonly set to $0.05 \mu S$. Whereas nowadays, with computerized scoring of EDR records, the definition of the minimum amplitudes has been set as low as $0.01 \mu S$ [10]. It is important to keep in mind, that choosing such a low value might lead to equipment related noise being scored as a response. After the peak deflection, the recovery begins. In this phase the electrodermal reading declines. The recovery is a much slower process than the rise. This is caused by the increase in conductivity of the corneum, elicited by sweat, in the time period following EDRs. There are certain way points, which are usually determined, e.g. the half time recovery (EDR rec.t/2), which is the time that passes until half of the amplitude has recovered. As the recovery proceeds the EDR is concluded.

Tonic Electrodermal Measures

The measures of the relatively long-term tonic EDA states can be divided into two basic principles, the skin conductance level (SCL) and nonspecific skin conductance responses (NS-SCRs). SCL refers to the level of conductance in the absence of phasic SCRs. To guarantee a distortion-free measurement of SCL, all event and artifact related SCRs have to be detected and removed. SCL is typically expressed in units of micro Siemens and computed as a mean of several measurements, taken during specific time periods.

NS-SCRs on the other hand are phasic increases in skin conductance that resemble the elicited SCRs. However, they are considered to be tonic components of the EDA signal. The reasoning behind this is the absence of a distinct stimulus, related to their occurrence. According to SCL, NS-SCRs can be recorded in periods without or in between a stimulus presentation, e.g. a resting phase. NS-SCRs usually are expressed in number of responses per time interval, most commonly per minute. As mentioned before it is important to define a threshold to determine which responses will be rated as such.

Psychological and Social Context of EDA

This section is based on a review of the psychological and social factors that have been shown to influence EDA, done by Cacioppo et al. (2007). Three different types of paradigm have been reviewed: (1) those that involve the presentation of discrete stimuli, (2) those that involve the presentation of continuous stimuli, and (3) those that involve examining the correlates of individual differences in EDA. The present section will briefly cover the first two types.

Effects of discrete stimuli

There are a number of stimulus attributes to which the SCR is sensitive, including stimulus novelty, arousal content, significance, intensity and surprise. Although it may be impossible to identify an isolated SCR as an "attentional" response or an "anxiety" response, it is however possible, to interpret the psychological meaning of a SCR by providing a strict experimental paradigm. The better controlled the experimental paradigm, the more conclusive the interpretation. If there is only one attribute of the stimuli changing during the experiment, such as intensity, elicited SCRs can be matched more precisely and therefore allow a better interpretation of the psychological process involved. For example, the International Affective Picture System (IAPS), which has been developed by Lang et al. (1998), consists of a variety of pictures that are rated for both their arousal-producing quality and their valence. The valence scale ranges from strongly positive to strongly negative pictures. SCRs elicited by the use of the IAPS have been found to be related to the arousal dimension, with responses increasing in magnitude as arousal rating increased for both positively valenced and negatively valenced pictures [8].

Effects of continuous stimuli

In contrast to the brief, discrete stimuli, as reviewed earlier, continuous stimuli are rather long-lasting and can be thought of as modulating changes in tonic arousal. In this

context SCL and the frequency of NS-SCRs provide the most useful measures of EDA, because they can be measured over long periods of time. There are certain continuous stimulus situation which will reliably produce an increase in EDA. One example that can be mentioned here is performing a task. Performing as well as anticipating almost any task will cause an increase of both SCL and the NS-SCR frequency. This has already been shown by the following studies, which have been reviewed by Cacioppo et al. (2007). Lacey et al. (1963) recorded palmar SCL during rest and during anticipation and performance of eight different tasks. They confirmed an increase of SCL in every task situation. According to the results the SCL rose by one μ S during anticipation and by another one or two μ S during performance, when compared to the resting level. Other findings suggest that situations in which strong emotions are elicited also increase tonic EDA arousal. Ax(1953) created genuine states of fear and anger in his subjects by causing them to believe to feel in danger of a high-voltage shock due to equipment malfunction or by treating them in a rude fashion. Both SCL and NS-SCRs rose during the fear as well as the anger conditions [8].

Conclusion

In conclusion, EDA serves as a sensitive peripheral index of sympathetic nervous system activity. As mentioned above, the eccrine sweat glands are entirely under sympathetic control and therefore increases in both SCL and SCR mirror tonic and phasic sympathetic activation. EDA provides for a relatively direct and inexpensive measure that comes with great utility and can be used as an reliable indicator of arousal and attention.

1.2.4 Electrocardiogram

Anatomical and Physiological Basis

The cardiovascular system consists of two main components, the heart, which functions as a pump, and the vasculature, as a distribution system, that together ensure a constant blood supply throughout the whole body. The heart provides a steady flow of oxygenated blood, by sending blood into the lungs (pulmonary circulation) and then to the rest of the body (systemic circulation).

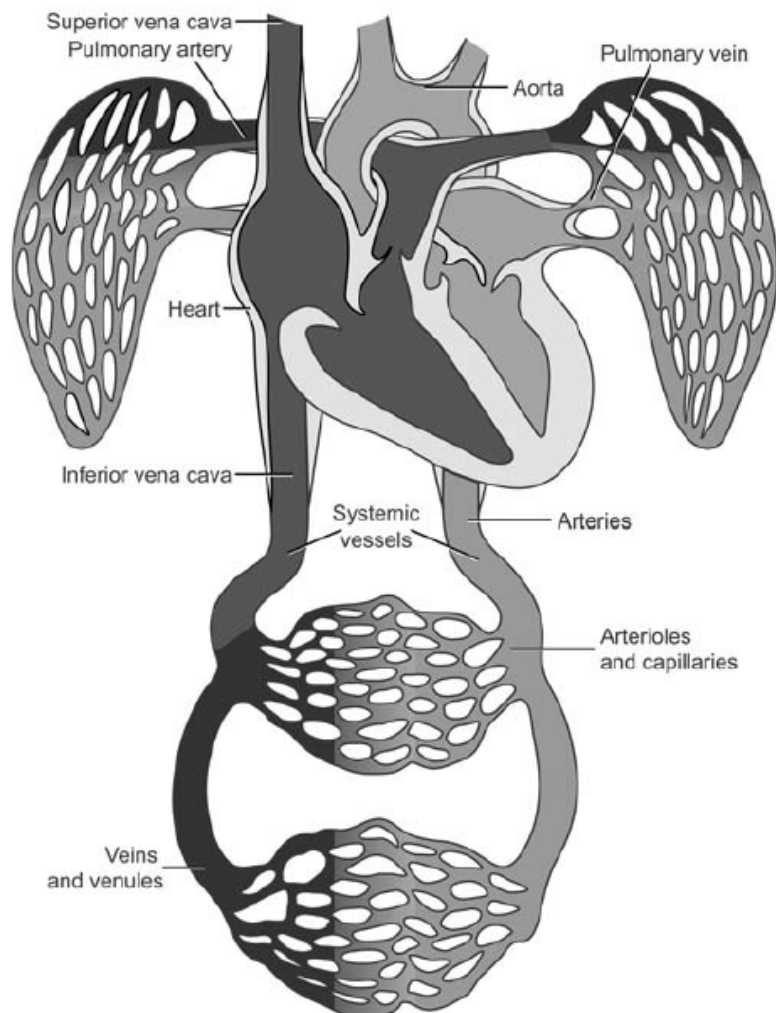


Figure 1.8: Ventral perspective of the systemic and pulmonary circulation. Lighter gray areas indicate oxygenated blood and darker gray areas indicate deoxygenated blood.

As can be seen on figure 1.8 the deoxygenated blood returns to the heart through the

superior and inferior vena cava. After passing the right atrium the venous blood reaches the right ventricle of the heart, from where it is pumped into the lungs for re-oxygenation purposes. Completing the pulmonary circulation, the oxygenated blood returns to the heart through pulmonary veins, reaching the left atrium first and finally the left ventricle. From here the blood is pumped into the aorta and distributed in the rest of the body. On its way to the periphery the blood passes through ever smaller vessels, starting with large arteries, which later branch into smaller arterioles and finally into capillaries. The capillaries are small, thin walled vessels from which oxygen, nutrients and waste products, such as carbon dioxide, are exchanged with the tissue. Leaving the capillaries, the blood returns to the heart again through the venous part of the systemic circulation. After passing the slightly larger venules the blood flows into increasingly larger veins until it reaches the vena cava and the circle closes.

The human heart can be divided into four chambers, two on either side. Each of the sides consists of an atrium at the top, or rostral, half and a ventricle at the bottom, or caudal, half. The heart contains three different types of cardiac muscle tissue, atrial and ventricular muscle fibers as well as specialized conducting fibers. The muscle fibers primarily serve the pumping function of the heart but also form a syncytium. This means, the tissue is electrically coupled in a way that allows for a rapid spread of depolarization along the longitudinal axis of the heart. There are two separate syncytiums, the atrial and the ventricular one, which are connected by an electrical conducting system. Although they are electrically connected it is crucial that both portions of the heart function as separate pumping units and all chambers are coordinated, in a way where the ventricular action is always triggered shortly after the atrial action.

This challenge is met by a special conducting system, formed out of specialized conducting fibers, which is embedded into the cardiac muscle tissue. The contraction of the heart can be triggered by the depolarization of two nodes of electrically active tissue, the first one being the sinoatrial (SA) node followed by the atrioventricular (AV) node. The SA node, serves as the pacemaker of the heart and is located inside the wall of the right atrium right beneath the entering point of the vena cava superior. A system of internodal, conductive fibers connects the two nodes. The depolarization wave is transported into the ventricles by passing the bundle of His, which branches into the left and right bundles and then transition into the Purkinje fibers. These fibers pass through the interventricular septum and deliver the depolarization into the rest of the ventricles.

The cardiac cycle is a term that describes all events that occur in the heart from one beat to the next (see figure 1.10). The cycle is divided into two main phases, the diastole and systole. During the systole the pumps and the blood is evacuated into the arteries, whereas the heart will be filled again during the diastole. The electrocardiogram (ECG) is the graphical representation of the electrical potential produced by the electrical current passing through the heart. It is recorded via electrodes positioned on the body surface and displayed in forms of so called waves or deflections [11].

The cycle starts with the depolarization of the SA node during the final stage of the diastole. The process of the depolarization wave passing through the atrial muscle tissue corresponds to the P wave of the ECG. Following the P wave is the atrial contraction,

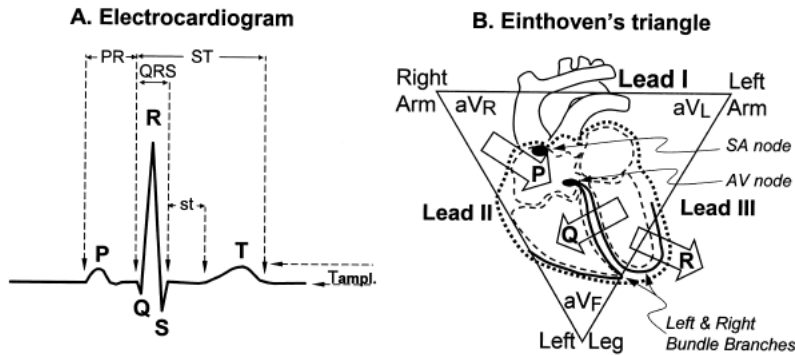


Figure 1.9: A: General morphology of the ECG showing P, Q, R, S, and T components, the PR, ST and QRS intervals, the st segment, and the T wave amplitude; B: The heart, conducting system, and Einthoven's triangle. Open arrows indicate the direction of propagation of electrical activation and the associated component of the ECG.

during which the QRS complex appears in the ECG. This complex reflects the contraction of the ventricles and the demarcation of the onset of the systole. During the contraction, the intraventricular pressure reaches levels high enough to close the AV valves, which are located between the atria and the ventricles. After the ventricular contraction has ended the ventricular pressure will start to drop again, eventually causing it to fall below the atrial pressure and allowing the AV valves to open and the blood to fill the ventricles. However, once the ventricular pressure exceeds the aortic pressure the aortic valve opens and blood is evacuated into the systemic circulation. In the latter part of the ventricular contraction phase the ventricles repolarize, creating the T wave in the ECG and initiating the relaxation of the ventricles as well as the onset of diastole.

ECG Measurement

As mentioned above, the ECG is a graph that represents cardiac electrical activity from one instant to another. The ECG pictures the heartbeat in the form of a time-voltage chart. The general study of ECGs, including its clinical applications and technological aspects, is called electrocardiography [12]. Accordingly, the device, used to measure and display the conventional (12-lead) ECG, is called an electrocardiograph. It records the cardiac electrical activity through electrodes, which are positioned selectively on the body surface. Current ECGs most commonly use disposable self-adhesive silver-silver chloride electrodes, which were traditionally placed on the limbs. These extremity leads can be represented by the Einthoven triangle (see Figure 1.9B). As illustrated there are six leads in total, three unipolar leads, which are taken of the right arm (aV_R), the left arm (aV_L) and the left leg (aV_F), as well as three bipolar leads, taken between I:

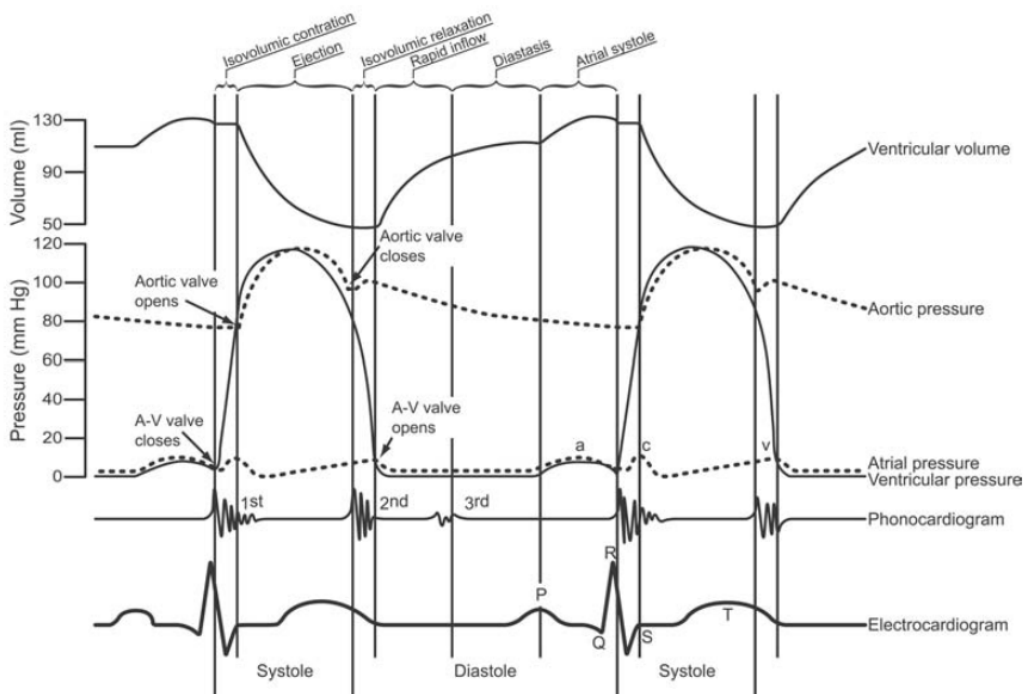


Figure 1.10: The graphic shows two full cardiac cycles for various aspects, which can be seen on the right.

left arm - right arm, II: left leg - right arm and III: left leg -left arm, with the right leg being the ground. Typically these leads are approximated by placing the electrodes on the torso instead of the limbs. In clinical cardiology, a series of unipolar precordial chest leads are usually added to provide a variety of distinct electrical perspectives on certain heart events. These leads start from the right lower peristernal region, with the first lead being labeled V1, and extend laterally to the left (V2-V6). However, for most psychophysiological applications a simpler configuration, such as lead II, will suffice as they still yield a large enough R wave [8].

ECG Signal Components

The present section is based on the work of Goldberger et al. (2017) and will briefly outline all components of an ECG signal. The clinical ECG graph consists of three different component types, waveforms, intervals and segments. Their distribution is specified by the 5-4-3 rule, which states that there are five waveforms (P, QRS, ST, T and U), four sets of intervals (PR, QRS, QT/QTc and RR/PP) and three segments (PR, ST and TP)[12].

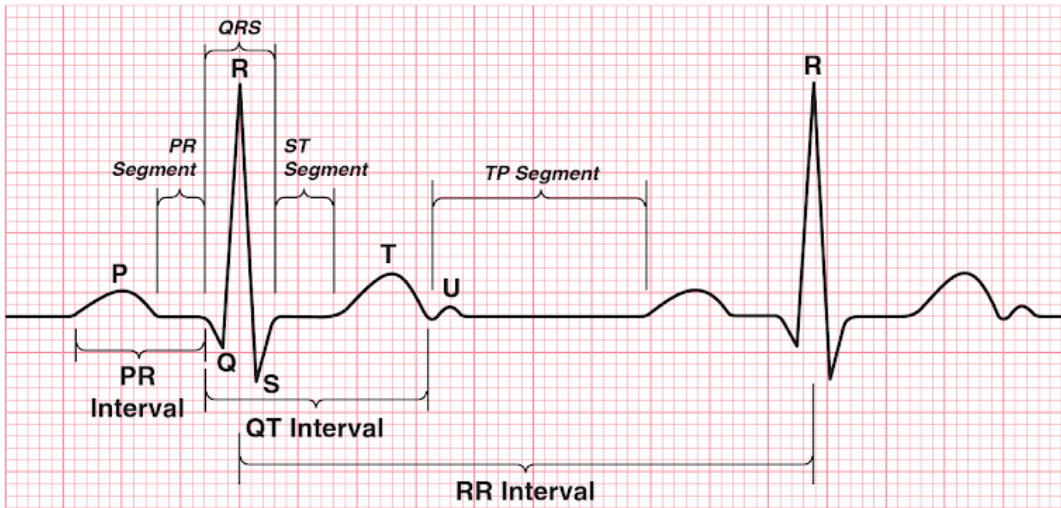


Figure 1.11: Summary of all major components of the ECG graph.

Waveforms

The five basic ECG waveforms are named alphabetically, starting with the P wave, which represents atrial depolarization. The QRS waveform, which is often referred to as QRS complex, represents the ventricular depolarization. The ST and T wave represent the ventricular repolarization, eventually resulting in the U wave depicting the final stage of said repolarization. The atrial repolarization is generally not observed, because of the small amplitudes of the atrial ST segment and atrial T wave. Together these waveforms represent a complete cycle of the electrical activity of the heartbeat.

Segments

As mentioned before there are three basic segments contained in the ECG graph, which are defined as the spaces between two waveforms. The PR segment is defined as the distance between the end of the P wave and the start of the QRS complex. It marks the start of atrial repolarization, which is continued throughout the QRS complex and ending during the ST segment. The ST segment spreads from the end of the QRS complex to the beginning of the T wave. TP segment connects the end of the T wave with the beginning of the P wave of the next cycle. This segment represents the electrical resting state and is typically used as a baseline reference for PR and ST deviation assessment in clinical diagnostics.

Intervals

Per definition intervals are parts of the ECG that include a minimum of one entire waveform. The PR interval is measured from the beginning of the P wave to the beginning of the QRS complex and is followed by the QRS interval, which lasts until the end of the same QRS complex. The QT interval is defined from the start of the QRS

complex to the end of the T wave. The RR interval is the last of the four and lasts for an entire heart cycle, starting and ending at a predefined point in the QRS complex, which is often referred to as the R point. It can be used to calculate the instantaneous heart rate (HR_i) in the following manor.

$$HR_i = 60/RR \quad , RR \text{ in units of seconds} \quad (1.5)$$

Heart Rate and Heart Period

The heart period (HP) is the time in milliseconds between two heart beats. It is usually determined by measuring the distance between two successive R spikes in an ECG, due to their prominence in comparison to the other components. The heart rate (HR) is a more common way when communicating heart activity. Typically the heart rate is given in beats per minute (bpm) and can be determined by calculating the reciprocal of the heart period.

$$HR = 60000/HP \quad (1.6)$$

There are incidents however, in which heart rate and period are not linear. As mentioned by Caciappo et al. (2007) "Berntson and colleagues (1995) reviewed literature across several mammalian species, including humans, showing that the relationship between changes in activity of the parasympathetic and sympathetic autonomic branches and heart period are more nearly linear than the relationship between activity in either branch and heart rate". This means that certain change in activation of either branch of the ANS will result in an equal change in heart period, whereas the same is not true for heart rate. It is important to mention that the change in heart period is independent from the baseline heart period at the time. For example, raising the stimulation frequency of the vagal nerve by 2 Hz in dogs, results in a change of 70-72 msec in heart period, regardless of the baseline heart period being either 875 msec or 350 msec. In contrast, applying a 2 Hz change in parasympathetic activation resulted in different heart rate changes for either baseline. Heart rate of dogs with a heart period baseline of 875 msec changed by 5.1 bpm and by 29.2 bpm for a 350 msec baseline [8]. Therefore the choice of the metric can heavily influence the outcome of an experiment. Bernston et al. (1995) recommended heart rate as the metric of choice when changes in cardiac functions are likely to be caused by autonomic effects and when those changes vary widely as a result of an experimental manipulation or between groups because errors caused by the nonlinear relationship between autonomic inputs and heart rate can be significant and result in misinterpretations of the data [8].

Heart Rate Variability

The oscillation in the interval between consecutive heart beats as well as the oscillation between consecutive instantaneous heart rates is called heart rate variability (HRV) (Task Force of the European Society of Cardiology the North American Society of Pacing Electrophysiology, 1996 ; from now on Task Force). Measures of the HRV can be divided into three general groups, the time domain methods, the frequency domain methods and non-linear methods. Time based methods determine either the HR at any given point in time, by calculating the HRi, or the intervals between successive normal complexes, by detecting the so called normal-to-normal (NN) intervals. Simple time-domain variables that can be calculated include the mean NN interval, the mean heart rate and the difference between the longest and shortest NN interval (Task Force, 1996). Frequency domain methods on the other hand decompose the overall heart period variance into specifiable frequency bands [8]. A common approach are power spectral density (PSD) analysis, which are based on a Fast Fourier Transform (FFT) of the HRV and provide basic information on how power distributes as a function of frequency. When considering only short time HRV recordings ranging from 2 to 5 minutes three major spectral components can be distinguished. There are very low frequency (VLF), low frequency (LF) and high frequency (HF) components [13]. The distribution of the power and the central frequency of each frequency band vary in regard to changes in autonomic modulation of the heart period. In general high-frequency HRV is mostly attributable to variations in the parasympathetic control associated with respiration and is commonly used as an index of vagal control of the heart [8]. Whereas low-frequency HRV's psychological significance remains a controversial topic. Contrary to the assumption of LF HRV being related to cardiac sympathetic activity it seems to rather reflect both sympathetic and vagal influences related to baroreflex mechanisms [14].

Non-linear phenomena are determined by a number of complex interactions of haemodynamic, electrophysiological and humoral variables, as well as autonomic and central nervous regulations [13]. Although a variety of techniques has been applied to determine non-linear properties no major breakthrough in the field of HRV analysis has been achieved yet.

1.3 General

1.3.1 Related Work

Virtual reality combines real-time computer graphics, body-tracking devices and high-resolution visual displays to create a computer-generated virtual environment. With their ability to immerse the user into a virtual mirror of the real world, virtual environments

are a powerful tool in clinical application, especially in the treatment of phobias [15]. Studies have shown anxiety disorders to be the most prevalent mental disorders [16]. Many consider exposure therapy the most effective form of treatment for specific phobias [17]. However that may be, considering the nature of certain phobias, such as fear of heights, exposure therapy involves a genuine risk of injury. Performing therapy in a virtual environment therefore can be a promising alternative to the conventional in-vivo exposure.

The efficacy of virtual reality exposure therapy (VRET) has already been demonstrated in the past. A study conducted on acrophobia compared two groups of student subjects. The first group received a graded VRET. Whereas students of the second group were added to a waiting-list as a control group. Results showed VRET to be more effective than no treatment [18]. A few years later, VRET was also found to be as effective as exposure in-vivo in a more recent work by Emmelkamp et al. (2002).

In addition to this using a virtual reality system can have a number of advantages over in-vivo exposure. First and foremost being the ability to conduct therapy inside a controlled and secure environment like a therapist's office for example. This also implies therapy being less time consuming and provides considerable financial benefits [19]. The possibility of having therapy in a more private scenario also increases the likelihood of acceptance in people that are too anxious or afraid of public embarrassment. A recent study exploring the acceptability of virtual reality exposure and in-vivo exposure in subjects suffering from specific phobias supports this hypothesis. When given the choice, 76% of the subjects chose virtual reality exposure over in-vivo exposure. In addition to this the refusal rate of 3% for virtual reality exposure was substantially lower than 27% for in-vivo exposure [20]. Further epidemiological studies have shown a lifetime prevalence of 28.5% for vHI and 6.4% for acrophobia alone and that only 11% of susceptible people were willing to consult a doctor [21] [4].

These results illustrate just how difficult and intimidating an in-vivo exposure can be to a phobic and how virtual reality exposure could help increase the number of people who seek therapy for phobias and therefore needs to be established in everyday clinical work. In recent years there has been a lot of research on virtual reality treatment for different phobias trying just that.

For example a controlled study by Rothbaum et al. on aerophobia (2000) as well as an open clinical trial on post-traumatic stress disorder (2001) and a study on agoraphobia by Meyerbröker et al. (2011), all of which yielded positive results [22] [23] [24]. Aside from these studies researching the general use of VRET, there also have been studies on ways to control the virtual reality. In a pilot study, Levy et al. (2016) explored the possibility of a remote-controlled virtual reality. After a trial session in a neutral virtual environment the patients received a total of six therapy sessions. The first three sessions were remote-controlled virtual reality exposure therapy (e-VRET) followed by three sessions in the presence of a therapist (p-VRET). E-VRET sessions were conducted without any contact to the hospital staff. The study showed that e-VRET not only is possible but produces results equal to p-VRET [25]. This inevitably leads us to the idea of a entirely independent VRET, which to some degree already exist on the market. This is an idea of which we shy away from. In regard to the possible harm that could

be caused by patients attempting to treat themselves instead of a receiving professional consultation. Assessing the mental state of a patient is essential for the success of the therapy. A task which usually falls to the hands of the psychiatrist, leading the exposure, and in most cases relies on a verbal communication between both parties. Returning to the topic of an e-VRET, intending to ensure the quality of our system we clearly have to provide some sort of substitute for this.

Past studies have shown a strong psychophysiological arousal in in-vivo exposure for different specific phobias [26] [27]. In a more recent work Diemer et al. (2015) also confirmed physiological arousal in subjects executing a virtual height challenge [28]. The study examined phobics and healthy controls in terms of subjective and physiological fear reactions resulting in a significant increase of subjective fear, heart rate and skin conductance level. Emmelkamp et al. (2001) also used psychophysiological measures to actively guide the therapy. To aid the therapist in deciding whether anxiety had diminished, the heart rate was monitored throughout the virtual reality exposure sessions using an ambulatory heart rate device. The actual heart rate was displayed continuously on a monitor. Based on reduction in the subjects subjective anxiety rating and heart rate, the therapist could decide to switch to an exposure scene with higher difficulty [29]. This method was found to be very well accepted by the therapists, for compensating the patient's low ability of introspection when experiencing anxiety or a panic attack. In conclusion, virtual reality exposure is a valid alternative to in-vivo exposure and can be used to efficiently treat people suffering from phobias, especially when paired with psychophysiological measurement.

1.3.2 Problem Analysis and Goals

In this section we will have a closer look at the preceding studies on phobia treatment, analyzing methods and show ways of improvement. There are two major conditions, which have to be met for an exposure therapy to be successful. The first condition is the ability to elicit fear in the patient. A task that as has been shown can be achieved by a number of virtual scenarios. However, past virtual reality environments exclusively featured either a single stimulus strength, a number of scenes with different stimuli, which required the user to change scenes in order to alter the difficulty of the exposure, and exposure scenarios with varying difficulty, which were presented in a certain routine. These methods may be sufficient for research purposes but to integrate them into actual therapy some alterations have to be made. For example, to fit the needs of a variety of patients, a virtual height challenge with only one intensity is highly insufficient. Whereas on the other hand a monotonous experience is unlikely to maintain a certain degree of activation over a number of sessions. In addition, frequent changes in scene will hurt the immersion of the patient and therefore might interfere with the treatment. In consideration of these arguments our goal was to design a virtual environment that features a progressive and seamless transition between a variety difficulties, and real-time adaption to the current needs of both patient and therapist. The second condition for

a successful therapy is to allow for emotional processing (see 1.2.2). This means that the effectiveness of the treatment is closely related to the fact how the patient perceives information during the exposure. It is necessary for the exposure to be long enough so the patient can habituate to the situation and receive corrective information. Thus, to optimize exposure time we provide the therapist with a steady stream of information in the form of a graphical presentation of skin conductance and heart rate variance. Our goal is to provide a system that features a closed loop of constant information flow.

2 Materials and Methods

2.1 Materials

All experiments and measurements were conducted within the facilities of Systems Neuroscience and Neurotechnology Unit, particularly the Green Lab, which is located at the Saarland University Hospital.

2.1.1 System Components

The virtual reality system is comprised of a number of components, some of which were created in the scope of a different thesis¹. Therefore, this section will focus on components that were built in the scope of the present thesis and delineate what is necessary to run the virtual reality system.

2.1.2 Hardware

HTC Vive

The Vive is a commercial virtual reality system that has been developed by HTC in cooperation with Valve and is composed of a Head-Mounted Display (HMD), a tracking system, called Lighthouse, and two controllers. Inside the virtual environment, which is presented to the user via the HMD, the user's position is tracked by the Lighthouse-System at all times, allowing for the user to explore the virtual environment. The Tracking system is composed of a minimum of two base stations, which are located at the edge of the intended tracking area, approximately 2m above the ground. In addition the controllers can be used to perform tasks and to interact with objects inside the virtual world. The Vive can be used in combination with any computer fitting the following minimum requirements.

¹This is a reference to the master thesis of Santhosh Nayak, a fellow student, contributing to the project.

System Requirements

- Graphics: NVIDIA GeForce™ GTX 1060 or AMD Radeon™ RX 480, equal or higher
- CPU: Intel™ Core™ i5-4590 or AMD FX™ 8350, equal or higher
- RAM: minimum of 4 GB RAM
- Video port: 1x HDMI 1.4-port or DisplayPort 1.2 or newer
- USB ports: 1x USB 2.0-port or newer
- Operating System: Windows™ 7 SP1, Windows™ 8.1 or newer or Windows™ 10

Tracking Space Requirements

To guarantee a satisfying experience a minimum room size of 2m x 1.5m with a maximum distance of 5m between base stations is suggested by the manufacturer.

BITalino

The BITalino (r)evolution Plugged kit is an innovative low-cost toolkit that was developed for rapid prototyping of wearable devices and biomedical signal acquisition. The main board, or BITalino Core, is comprised of major components, the Microcontroller (MCU) Block, the Bluetooth Block, the Power Block with the device's own LiPo battery and the UC-E6 connectors. The MCU features 12 ports, which are divided into 8 analog and 4 digital ports. Of the 7 separately included BITalino sensors, which are connected via cable, only the EDA sensor and the ECG sensor were used. The data is recorded with one of the 4 preset sampling rates and then sent to the user's computer, via a Bluetooth connection. The BITalino is supported by a number of platforms, such Matlab and Unity, allowing for easy implementation in almost any data acquisition process.

Specifications

- Analog Ports: 4 in (10-bit) + 2 in (6-bit) + 1 auxiliary in (battery) + 1 out (8-bit)
- Digital Ports: 2 in (1-bit) + 2 out (1-bit)
- Sampling Rate: 1, 10, 100 or 1000Hz

FUNCTIONAL BLOCKS

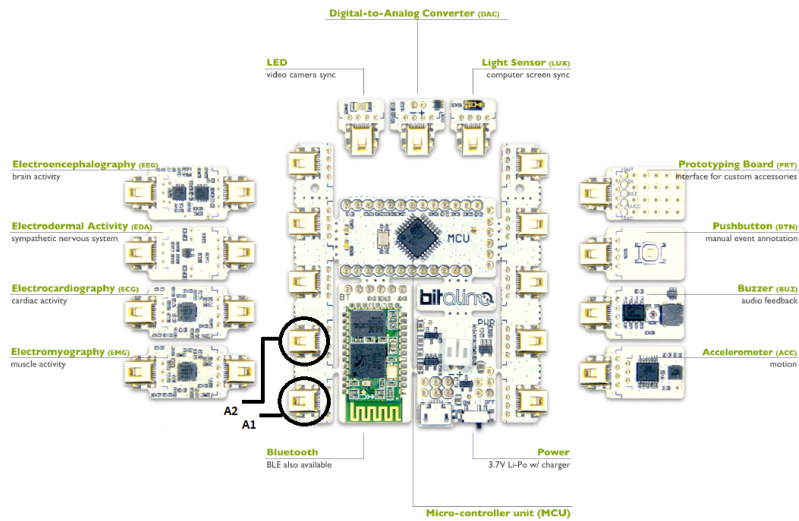


Figure 2.1: Graphical overview of the BITalino device including all functional blocks.

- Communication: Bluetooth
- Sensors: ECG, EDA
- Size: 100x65x6mm
- Power Supply: LiPo battery (500mA, 3.7V)

Accessories

- 1x EDA Sensor
- 1x ECG Sensor
- 1x 3-lead cable
- 1x 2-lead cable
- 2x UC-E6 to UC-E6 sensor cable
- pre-gelled electrodes

VR Unit (VRU)

VRU is the expression given to the computer, which is used to run the Unity software and power the HMD while the system is in use. It is to mention that the performance of the HTC Vive, in some degree, is reliant on the CPU and GPU of the VRU. Therefore exceeding the minimum requirements, although involving higher cost, has proven to be beneficial for the user experience, especially when the used virtual environment relies on realistic real-time lighting effects. On a monitor, which is connected to the VRU, the virtual world, as perceived by the HMD, is displayed for the user to see. However, while the system is in use, the software that is run on the VRU is controlled by a separate computer. Therefore it is essential that the VRU is able to connect to the internet. Alternatively a local network can suffice given one of the following conditions is met:

- a) the CMU (see [2.1.2](#)) is located in the same local network as the VRU
- b) the functions of VRU and CMU are handled by a single computer²

Control and Measurement Unit (CMU)

In the early design phase the CMU was conceptualized as a part of the VRU, but it was then separated in regard to its intended use as a mobile control device for the therapist during the therapy. However, in our experiment a Laptop served as CMU. The CMU enables the user to submit orders to the VRU, control the BITalino, as well as to view the preprocessed Data. To find detailed explanations to the functions mentioned above, see [2.2](#).

2.1.3 Software

As mentioned in section [2.1.2](#) the data acquisition is handled by a separate computer. However, all programs were designed to function on any device, capable of running the software in this section.

Unity

Unity is a game development platform, which can be used to create high-quality 3D games and deploy them across a variety of platforms, mobile phones, tablets and desktop

²If this variant is used, a Bluetooth adapter is required to connect to the BITalino device.

computers. The user is enabled to directly target a VR device through the implemented Unity VR Software Development Kits (SDK). The VR environment is built by creating game objects, such as structures and lights, and placing them inside a three dimensional virtual space or importing prefabricated assets from the Asset Store. Each game object can be equipped with a number of components to fit the user's needs. One of the most important aspects to the Unity platform is its scripting API that gives the user control over the game environment. This is accomplished by C# scripts, which are created in Visual Studio 2017 and then attached to the specific game objects. As a game development platform Unity naturally is provided with an extensive networking environment, including UDP and TCP/IP, which can be used for communication with external devices. In addition the support, offered to the user in form of the Unity Manual and Scripting API as well as the Asset Store, is sufficient to allow even non-professionals to create their own projects.

Matlab

Matlab is a software, which was created to solve mathematical problems. It was used for data acquisition and processing as well as feature extraction from the measured signals.

2.1.4 Virtual Environment

As mentioned earlier there are two major requirements that must be met to successfully treat phobias with virtual exposure, fear elicitation and emotional processing. To elicit fear in the subjects we have to ensure that adequate stimuli are offered in our virtual environment. We therefore have implemented three different ways to adapt the difficulty of our virtual height scenario. The virtual environment was designed around the concept of a descending floor inside a closed room. In the default configuration, which is shown in figure 2.2, a neutral environment is provided.

This configuration is used at the start of the session to conduct baseline measures and to allow for acclimation to the virtual reality. The first stimulus that is presented to the patient is the opening of the floor, which is shown in figure 2.4. Initially the floor was programmed to open completely. This was later adapted in regard to a recommendation by the psychiatry department. It was suggested that the ability to gradually move the floor to the side and therefore provide a form of minimal stimulation could be particularly useful in the treatment of very severe cases of acrophobia. Thus, two additional steps were implemented at the one third and two third mark of the full opening distance.

The actual height challenge as well as the two remaining stimuli are revealed once the floor has been opened up. The patient is then confronted with a narrow bridge located



Figure 2.2: A side view of the VR room in its default configuration.

above a descendable platform that is initially positioned 1m below floor-level (see 2.4, D). During therapy patients are asked to cross the bridge in order to confront their fear. A task, which in this state of the virtual environment, is considered to be of a lower difficulty. However, the difficulty can be adapted to each individual by alterations made to the strength of the primary stimulus, the depth. The platform can be lowered to a depth of up to 40m, enabling a degree of stimulation that could hardly be achieved in in-vivo exposure. But there are also precautions to be made to guarantee that the full extend of this stimulus can be perceived by the patients. For instance there are no natural light-sources in a closed room scenario. Therefore the virtual room has to be equipped with an operant lighting system. We have applied 4 ceiling lamps that each are featured with 2 different light-sources, a point and a spotlight. Point lights are located at a certain point inside the virtual space and send out light, which is equally distributed, in all directions. The intensity of the eradicated light is diminished with increasing distance to the source, eventually reaching zero at the a specific range, which was set to 13m. We have used point lights to simulate the natural patterns of light in close proximity to a big surface lamp. The glow of the light bulb itself was recreated by using a material property called emission, causing light to be emitted directly from an object's surface to which the material has been applied. Spotlights too have a specified location and range but are used to illuminate a constrained angle, resulting in a cone shaped region of illumination. In addition to the previously mentioned range specific intensity drop off, the intensity of the spotlight is reduced from the inside to the outside of the light cone, causing a fade effect in the outskirts region, the so called penumbra. We have used spotlights with a range of 13m and an angle of 165 degrees to light the room as well as the initial section of the pit. As the platform is lowered beyond this range it is obscured by shadows and becomes less visible. Therefore we have implemented additional light-sources that are activated and deactivated according to the current platform position. Thus, the platform



Figure 2.3: A top view of the VR room in its default configuration.

is sufficiently illuminated at all times (see 2.5, C and D).

In figure 2.5 four different depths, subsidiary for four stimulus intensities, are displayed: A = 1m, B = 8m, C = 25m and D = 40m. It has to be mentioned that those depths only were chosen to illustrate different therapy difficulties whereas the depth can be freely changed in steps of 1m. Earlier we have talked about the immersion being disrupted by changing scenes during the session. To counter this phenomena, we have programmed the transition phase between difficulties to be smooth and gradually instead of the floor being abruptly teleported to the new target location. The third available method of increasing the difficulty is an alteration to the width of the bridge. This also was implemented after a suggestion of the psychiatrists involved, improving the adaptability of our system. Similar to the opening of the floor we have decided for a total of four different widths, ranging from 25cm to 1m (see 2.6).

As full control is given over these three variables the therapist is enabled to adjust the exposure a every degree of fear. The methods that were used to enable control of the virtual environment are explained in section 2.2.3.

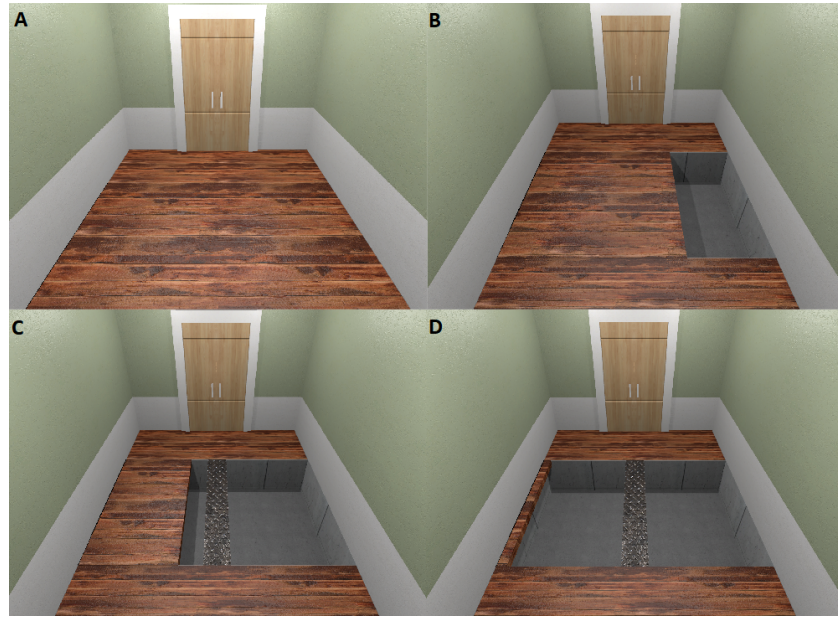


Figure 2.4: Comparison of the different stages of floor opening.

2.1.5 Virtual Reality Setup

To display the virtual environment, a powerful computer(Intel(R) Core(TM) i7-3770, 3.4 GHz and 8 GB RAM) and an Nvidia GeForce GTX 1080 graphics card with 8 GB of dedicated memory (GDDR5X) were used in combination with the HTC-Vive Head-Mounted Display (HMD). The Dual AMOLED displays (3.6" diagonal) of the HMD provided for a high-resolution presentation of the virtual world, with 1080x1200 pixel on each eye. The distance between the pupils was manually adjusted for each participant by means of a knob on the HMD to guarantee clear vision. Two base stations of the Lighthouse system were positioned in opposing corners at a height of roughly 2 m. Due to limited space, the exposure area was restricted to an area of 3.5 by 3.5 meter. The program, which was used to remotely control the virtual environment, was written with the Matlab software version R2015a and run on a Laptop (Intel(R) Core(TM) i5 6200U, 2x2.3 GHz and 8 GB Ram). The virtual environment was run on the desktop computer, using Unity version 5.6.1f1 personal. Both machines were connected through a closed network. We have used the BITalino device to record the physiological data and send it to our Laptop via a Bluetooth connection. We have chosen this device primarily for the convenience of wireless data transmission, higher maneuverability and less distraction for the patient.

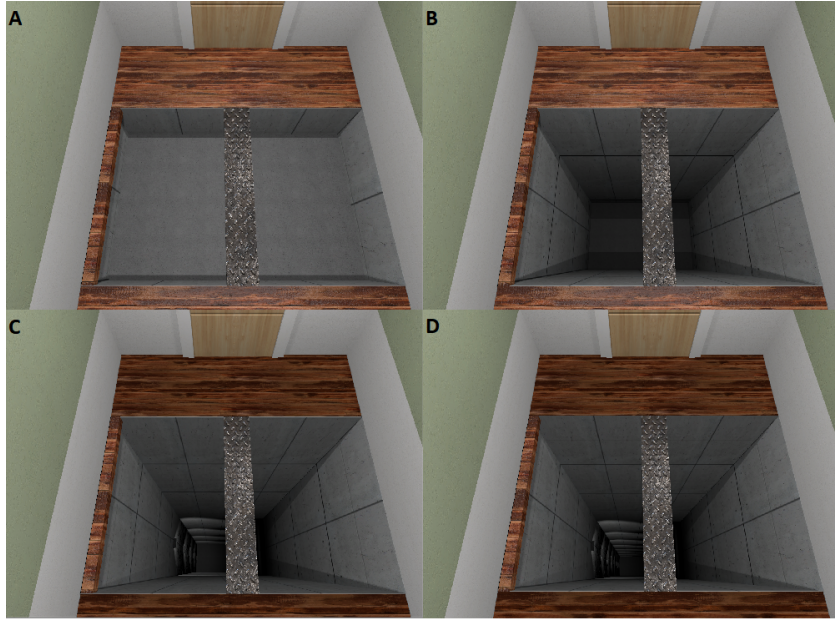


Figure 2.5: Illustration of 4 different platform position.

Closed Loop Information Flow

The key concept of our system was the adaptability of the virtual experience to the therapist standards as well as the individual standard. To achieve our goal we built our system in a way that information is constantly exchanged between the single components. The setup is composed of four major components that can be divided into two groups according to their function. Either the information is delivered to the subject (VRU and HMD) or retrieved from the subject and presented to the user (CMU and BITalino) (see figure 2.9).

The virtual environment was run on the VRU and presented to the subjects through the HMD. Inside the virtual environment the fear triggering stimulus was applied, causing a sympathetic reaction in the subject. This reaction was measured by the BITalino device, in the form of an ECG and GSR signal, and then sent to the control and measurement unit (CMU) via Bluetooth. Afterwards the data was processed by the CMU and displayed, in real-time, for the user to evaluate. Simultaneously the virtual world was displayed to a monitor, which allowed the user to see the perspective of the subject during the exposure. Based on the visual input, a decision to alter the virtual experience could be made by the user. This information was then submitted to the VRU, causing the virtual environment to react accordingly and therefore closing the information loop.

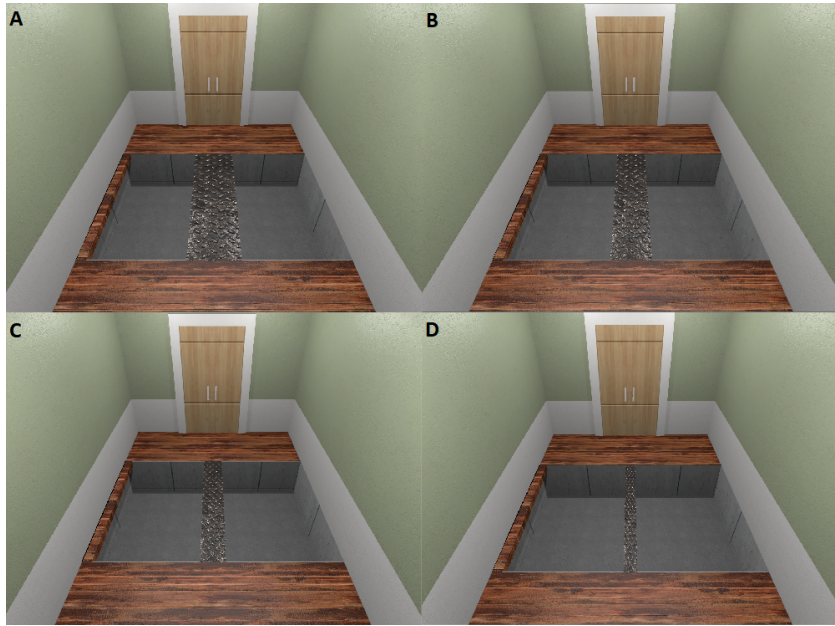


Figure 2.6: Comparison of the different widths of the bridge.

2.2 Methods

2.2.1 Participants

In total a sample 11 able-bodied individuals participated in our virtual reality experiment. The sample consisted of 6 men and 5 women aged between 23 and 54 years (median age: 27), of which 9 were right handed. When asked, 54.5% replied to never have experienced fear of heights or virtual reality in their life. All subjects volunteered to participate and gave their verbal consent to the use of their data in the present thesis. The subjects had no known conditions that may have affected their ability to perform the required tasks. However, 3 subjects reported to have a disposition to palmar sweating. Further, 9 subjects stated that they were feeling relaxed and 2 reported to be slightly nervous.

2.2.2 Procedure

At the start of the experiment the subjects had to answer a short questionnaire concerning personal information, their general attitude towards as well as their experiences with virtual reality and heights. Afterwards the participants were given a small set of directives for the experiment. They were asked to walk slowly at all times and not cover the motion sensors on the HMD with their hands. Further, they were told to wait for instructions before moving and to avoid unnecessary arm movement in order to minimize



Figure 2.7: Photograph of the experimental setup, located in the Green Lab in the University Hospital Saarland in Homburg. View on the control desk.

motion artifacts. We then proceeded by placing the electrodes on the subject's hands and connected them to the BITalino device. After the device was safely stored on the subject's body and the electrode cables were fixated the HMD was put on. We then adjusted the braces to each individual's head, ensuring optimal fit and thus concluding the subject preparation.

For the baseline recording, which lasted 4 minutes, the subjects were sitting on a chair inside the tracking area, allowing them to familiarize themselves with the virtual environment while being measured. Immediately after, the participants were instructed to move to the starting position. The virtual exposure was conducted in a circular pattern. Each cycle was lead by a short waiting period, in which the virtual reality was altered. Once the alteration was completed the subjects were given a signal, upon which they should move to the opposite side of the room and return back to the default position. In addition they were asked to look down every time they crossed and to stand still at times, while doing so. In the beginning of the exposure routine the floor was gradually opened in front of the subject (see 2.4), with a delay of 10 seconds between each step. Once the floor was fully opened the default exposure setting of 1m depth and a bridge size of 1m was revealed and the first cycle executed. For the second cycle the platform was lowered to 10m depth and the bridge size was reduced by 50cm. In the third cycle we set the virtual environment to the maximum difficulty setting, with a depth of 40m and a bridge size of 25cm. In the next two cycles the two parameters remained constant. However, for each crossing the lighting was changed to a different color, including red,



Figure 2.8: Photograph of the experimental setup, located in the Green Lab in the University Hospital Saarland in Homburg. View on the exposure area

blue and green. For the last crossing the color was changed back to the white default color. Once the subject had returned to the starting position the floor was gradually closed, thus completing the exposure. To finalize the experiment the HMD as well as the BITalino were removed and the subjects were given a second questionnaire, in which we asked them to rate their experience.

2.2.3 Virtual Reality Control

One of the major challenges, we were confronted with during this project, was to find a method that would allow for a reliable information transport between VRU and CMU. We have decided on a TCP/IP solution for this problem. This allowed for a loss-free data transmission between the two terminals. We used Microsoft Visual Studio to create a server in form of a script that reads incoming data streams, sent to the VRU's IP-address. The server was programmed to accept data from any client sending data to the specific port 8632. The data, contained in the stream, could only be read in sequential blocks. These blocks then had to be encoded into a sequence of bytes. Finally, by using specific converting methods for each data type, the information was extracted from the byte array and stored into the assigned variables. Since the script was attached to a game object

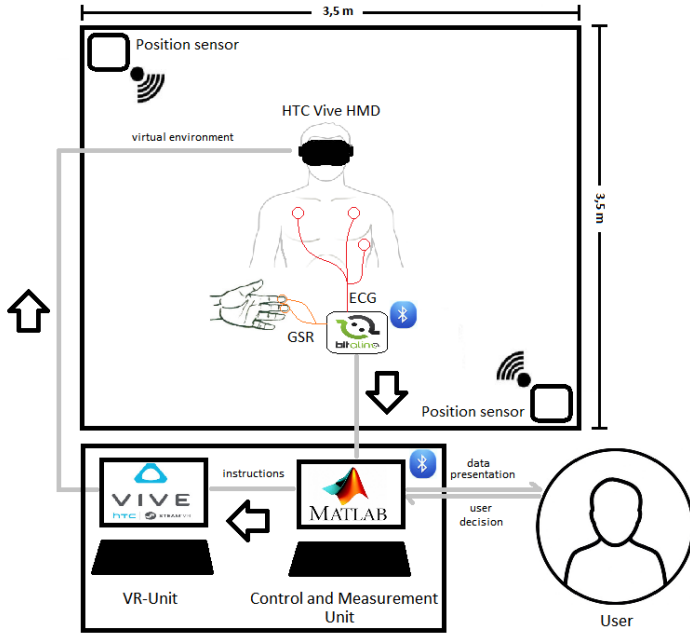


Figure 2.9: Closed-loop virtual reality system. The grey line illustrates the closed loop information flow.

inside the Unity environment we were able to make these variables accessible to the rest of the virtual reality and thus control certain game objects, such as the floor or the lighting. To control game objects or more precisely a certain aspect of them additional scripts were needed. These control scripts were designed to access the respective component of the game object we wanted to control and frequently update the component's variables with the values retrieved from the server script. For example if information was sent to lower the platform, the associated script would load the position variable of the transform component of the platform and override the current value with the new value, which was imported from the server script. Once this happened the changes to the game objects were immediately applied and therefore the virtual experience was altered.

As mentioned earlier the server was built to accept data from any client. However, one additional condition had to be met to guarantee the information could be understood by the server. The data had to be sent as an 8-bit coded array, containing all 12 variables in a specific order. During the development phase the data was sent from the CMU, using Matlab. Similar to the Unity server we have created a Matlab client that allowed the user to enter the desired values and then automatically built and sent the data array. In

the experimental phase of the project, the VR was controlled using a web application connected to a server structure, which was also handling the capture of the physiological data ³.

2.2.4 Data Acquisition

We obtained 100Hz ECG and EDA measures for the entirety of the experiment, using the BITalino (r)evolution. The sessions lasted approximately 11 minutes, consisting of a 5 minute baseline measurement and an exposure measurement, which lasted 7 minutes on average. For EDA two electrodes were placed on the distal phalanges of the non-dominant hand as well as three electrodes for ECG, which were placed on the palmar surface of both hands(see 2.10). The data was transmitted to the CMU, which was located in close proximity to the experiment area (2-3m), using a Bluetooth connection, and saved in text format (.csv). Afterwards the data was processed for further evaluation, using Matlab.

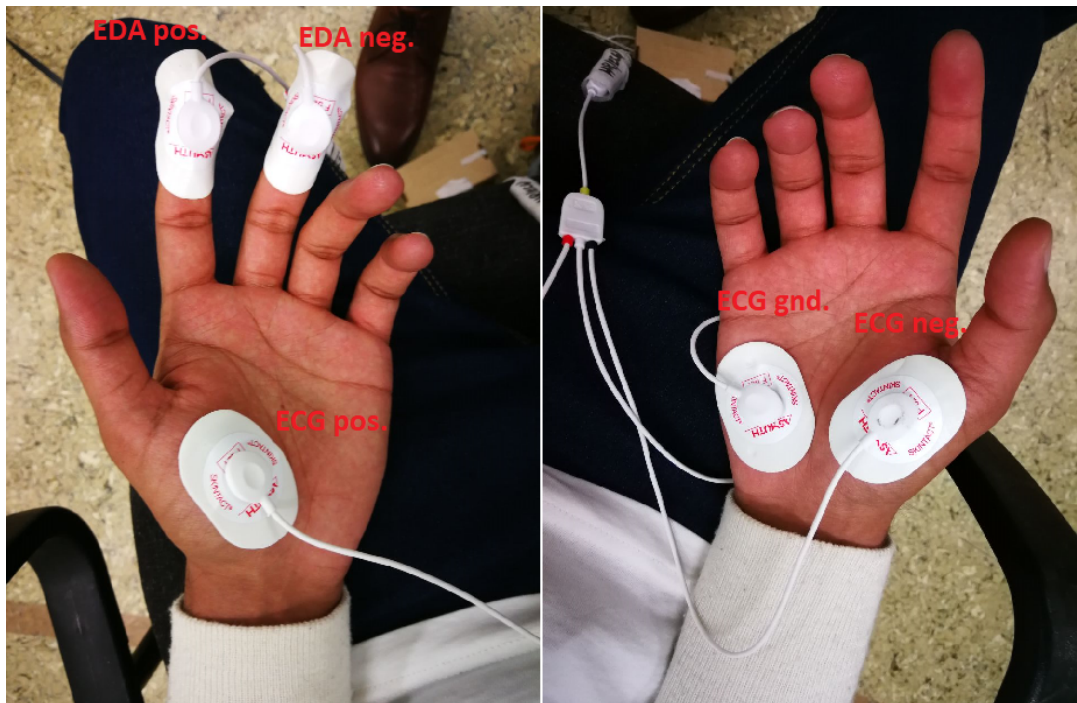


Figure 2.10: Example for electrode placement on a right handed subject.

³This application as well as the server have been created in the scope of mister Nayak's master thesis and therefore will not be described any further.

2.2.5 Data Processing

The present section covers all methods that were applied to the measured data in preparation for the feature extraction. We have divided these methods into two groups, the general processing, which was applied to both data sets and the individual processing, which includes specific modifications to each data set.

General Processing

The initial step was to import the text file, containing the saved data, into our Matlab program. The recorded raw data was then extracted and stored into a one-dimensional array, allowing for further editing. The second step was raw data adjustment, where we converted the data, sampled as 10-bit values from channels A1 and A2 of the BITalino device (see 2.1), for EDA and ECG respectively, into units of micro Siemens for EDA and milli Volt for ECG. The adjustment was achieved by applying the transfer functions given in the sensor's data sheet.

$$ECG(mV) = \frac{\frac{ADC}{2^n} - \frac{1}{2}}{G_{ECG}} \cdot VCC \cdot 1000 \quad (2.1)$$

This process is shown in the equation above. To convert the sampled raw data (ADC) into units of mV, we had to include the operating voltage (VCC) of 3.3V and the sensor gain (G_{ECG}) of 1100 as well as the number of bits of the channel (n) into our calculations. According to this, we also made adjustments to the EDA raw data, resulting in units of micro Siemens (see 2.2). Again the sampled raw data, operating voltage and number of bits were used as ADC, VCC and n, respectively.

$$EDA(\mu S) = \frac{\frac{ADC}{2^n}}{0.132} \cdot VCC \quad (2.2)$$

The adjusted signals had to be filtered to ensure quality feature extraction was possible. Therefore we have analyzed the signal in regard to its frequency components using a fast Fourier transform (FFT) algorithm 2.4. The discrete Fourier transform (DFT) was computed with the predefined Matlab function `fft` (see 2.3), which returned the n-point DFT for a time domain signal vector X. To increase the performance of the fft we have specified the transform length n as the power of 2 value closest to the signal length L. We then defined the frequency domain (0Hz-50Hz) and plotted the unique frequencies P.

$$Y = fft(X, n) \quad (2.3)$$

$$Y(k) = \sum_{j=1}^n X(j) W_n^{(j-1)(k-1)} \quad (2.4)$$

$$X(j) = \frac{1}{n} \sum_{k=1}^n Y(k) W_n^{-(j-1)(k-1)} \quad (2.5)$$

Where

$$W_n = e^{(-2\pi t)/n} \quad (2.6)$$

is one of n roots of unity.

The result was a frequency domain representation of the raw signal data, according to which the noise filters were designed. An example of a typical EDA measure is shown in figure 2.11. Using the FFT we were able to locate noise frequencies, such as the 50 Hz power line interference, and potential movement artifacts in the higher frequency areas, in foresight of the later filtering of the data (see figure 2.12).

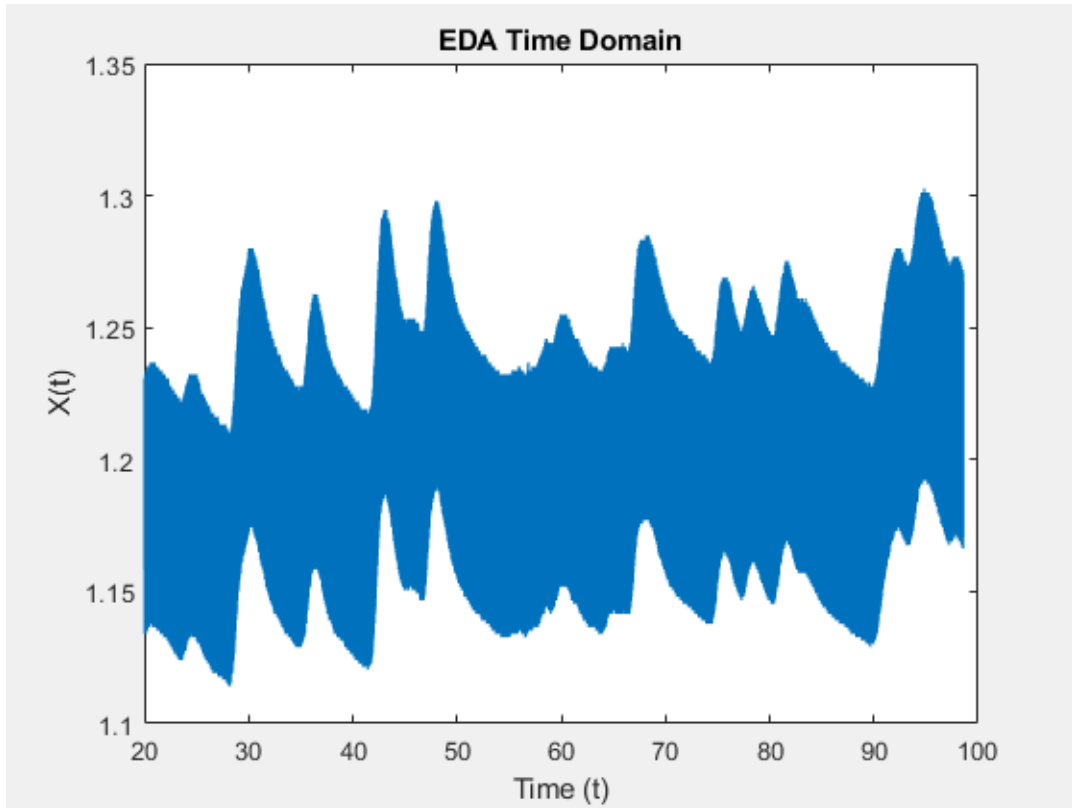


Figure 2.11: Raw data of an EDA measurement.

Once the filters were applied we cut off the first and last 10 seconds of each signal to eliminate eventual distortions or artifacts caused by the removal of the BITalino device.

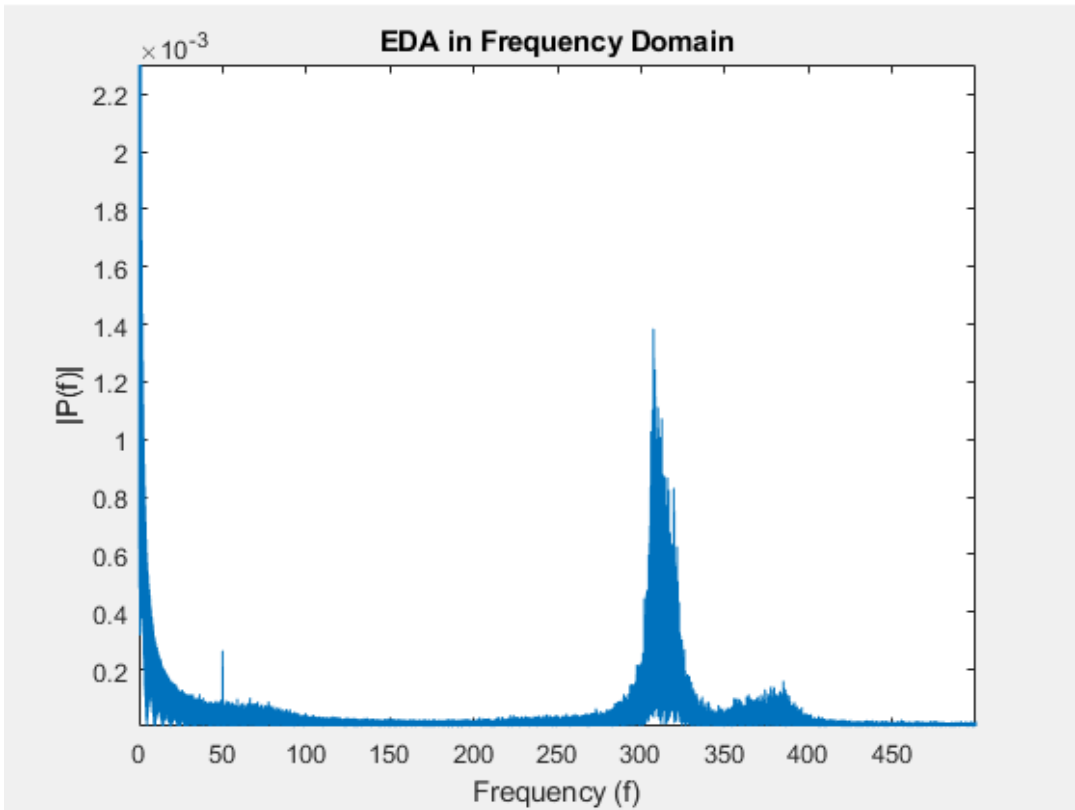


Figure 2.12: FFT of an EDA raw data set.

This was done by removing an equivalent number of samples from, both the start and the end of the data array. The number of samples was calculated using the following equation, with N = number of samples, F_s = sampling frequency and t = removed time interval.

$$N = F_s * t \quad (2.7)$$

ECG Processing

Our main goal was to enhance the ECG signal for optimized feature extraction, particularly Heart rate (HR) and heart rate variation (HRV). Therefore we had to reduce the noise in our signal by removing muscle noise, which most commonly occurs at approximately 40Hz, the effects of a possible DC drift and power line interference, while preserving the information bearing frequencies for QRS-detection of 5-15Hz [30] [31]. First, we took measures to remove DC drift from our signal, using the inbuilt Matlab function *detrend*. This function removed the best straight-line fit, which was created by computing the least-squares fit of a straight line or composite line for piecewise linear trends, from the data vector x and returned it in y (see 2.8). In the next step we analyzed the signal in regard to its frequency components using FFT (see 2.2.5).

$$y = \text{detrend}(x) \quad (2.8)$$

Although the frequency analysis did only in few cases show a 50Hz spike, we applied a notch filter with a notch frequency f_0 of 50Hz and a notch width of 0,1Hz to eliminate the 50Hz hum from our signal. We then used a bandpass filter to reduce the influences of muscle noise, baseline wander and T-wave interference. According to the well established Pan-Tompkins algorithm [30] we chose a Butterworth filter with a passband (W_p) of 5-15Hz to maximize QRS energy. The best results were achieved in combination with a stopband of 0.5-45Hz (W_s) and a passband ripple (R_p) of 1dB as well as a stopband attenuation (R_s) of 50dB. The filter order was calculated using the Matlab function *buttord* (see 2.9). It was designed to return the lowest order (n) of the digital Butterworth filter with no more than R_p dB of passband ripple and at least R_s dB of stopband attenuation. W_s and W_p , respectively the stopband and passband edge frequencies of the filter, were normalized from 0 to 1 by dividing them by the Nyquist frequency, with 1 corresponding to π rad/sample. We then used the *butter* function (see 2.10), a five step algorithm, to calculate the transfer function coefficients (b, a) for our digital bandpass filter of order n and the normalized cutoff frequencies W_n . Using yet another inbuilt function with the name *tf2sos* (2.11) we created a matrix (sos) in second-order section form with a gain (g) that is equivalent to the digital filter represented by the transfer function coefficient vectors (b, a), and therefore completed the filter building process. To apply the filter we have decided on the *filtfilt* function that performed zero-phase digital filtering by processing the signal data, in both the forward and reverse directions. More information on the matter, or the single algorithm steps can be found on the Matlab Documentation page under the topics *butter*, *tf2sos*, *filtfilt* [32].

$$[n, W_n] = \text{buttord}(W_p, W_s, R_p, R_s) \quad (2.9)$$

$$[b, a] = \text{butter}(n, W_n, ftype) \quad (2.10)$$

$$[sos, g] = \text{tf2sos}(b, a) \quad (2.11)$$

EDA Processing

Similar to the ECG filtering procedure we started by removing the power line interference, using the same notch filter that was described in the previous section. We then applied a digital low pass filter with a passband frequency of 1Hz as well as a stopband frequency

of 3Hz, a Rp of 1dB and a Rs of 60dB. This yielded satisfying results with adequate signal information and minimum to no noise.

2.2.6 Feature Extraction

Heart Rate and Heart Rate Variation

Heart rate (HR) is the speed at which the heart beats and is typically measured in beats per minute (bpm). Therefore the most significant step in the process of computing the HR is to determine the exact number of contractions of the heart in a certain time interval. This was done by detecting the R-peak of every QRS complex. Upon an initial inspection of the filtered ECG data it became obvious that before we could attempt to locate the R-peaks in our signal we had to make further preparations. We decided to normalize our signals to values between 0 and 1, using the equations below on every signal point ($signal_{ECG}$) inside the data array and therefore increasing the distance between R-peaks and P as well as T components. We subtracted the minimum value of our ECG signal ($signal_{min}$) and divided⁴ the result by the magnitude of our ECG signal ($signal_{mag}$).

$$signal_{mag} = |signal_{max} - signal_{min}| \quad (2.12)$$

$$signal_{norm} = (signal_{ECG} - signal_{min}) ./ signal_{mag} \quad (2.13)$$

This method yielded mostly positive results (see 2.13 and 2.14). However, on a small number of trials the effect of normalization was negated by high amplitude artifacts. To counteract this phenomena we applied an amplitude "cutoff" at 1mV as well as -0.2mV, by advising the value 1 to every amplitude above or equal to 1mV and accordingly the value -0.2 to every amplitude below or equal to -0.2mV⁵.

⁴./ is a form of division specific to Matlab, implying that the division is applied to each element of $signal_{ECG}$ individually.

⁵Please note that the main objective of normalization was solely the maximization the R-peak prominence, therefore neglecting authentic amplitude representation

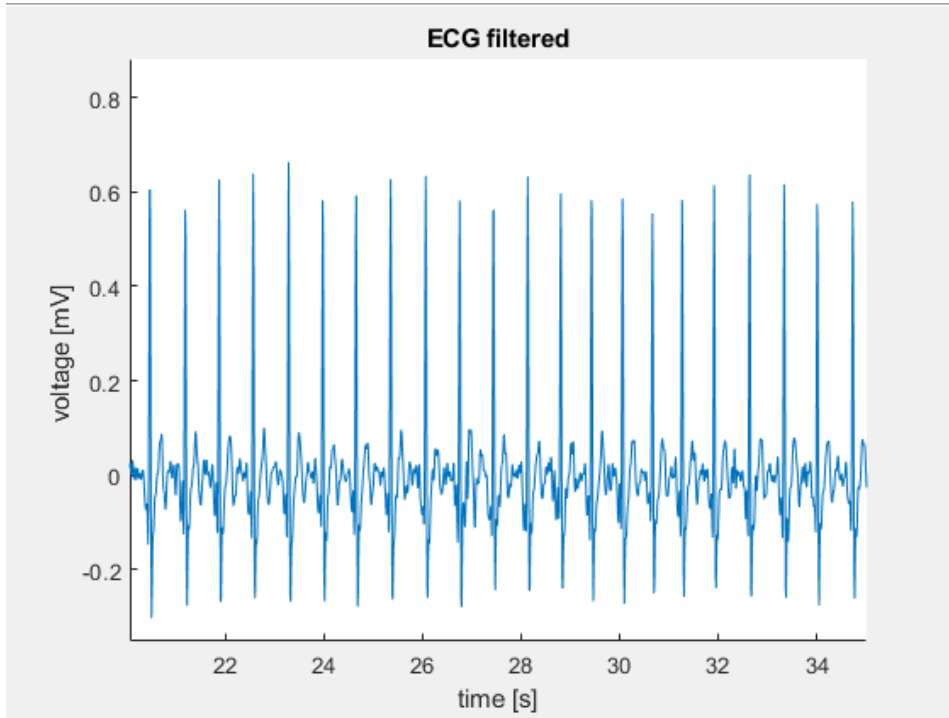


Figure 2.13: Graph of a filtered ECG signal segment with amplitudes varying around 0.6mV.

We then used the `findpeaks` 2.2.6 function to localize the R-peaks in our normalized signal. This function returned a vector with the local maxima (`pks`) of the input vector (`signalnorm`) together with an indices vector (`locs`) storing peak occurrences.

$$[pks, locs] = findpeaks(signal_{norm}, 'MinPeakProminence', p, 'MinPeakDistance', d)$$

Additionally a threshold for peak prominence (p) of 0.25 was applied to guarantee only those peaks that have the relative importance of p were returned. Together with a minimal peak distance threshold (d) of 31, which caused the algorithm to ignore smaller peaks in an interval, equal to the highest permitted heart rate (193bpm), around the detected R-peak, we reduced the false detection of P and T waves significantly. The maximum heart rate was calculated by subtracting the median age of our subject group of 27 from 220.

Peak indices were returned in units of samples and therefore had to be converted into units of seconds for further calculations. This was achieved, solving 2.7 for t. Afterwards we determined RR-intervals by calculating differences between adjacent elements of the indices vector (`locs`). As a second instance of artifact filtering we only accepted RR-intervals in the range of 0.310 seconds and 1.2 seconds, representing the highest

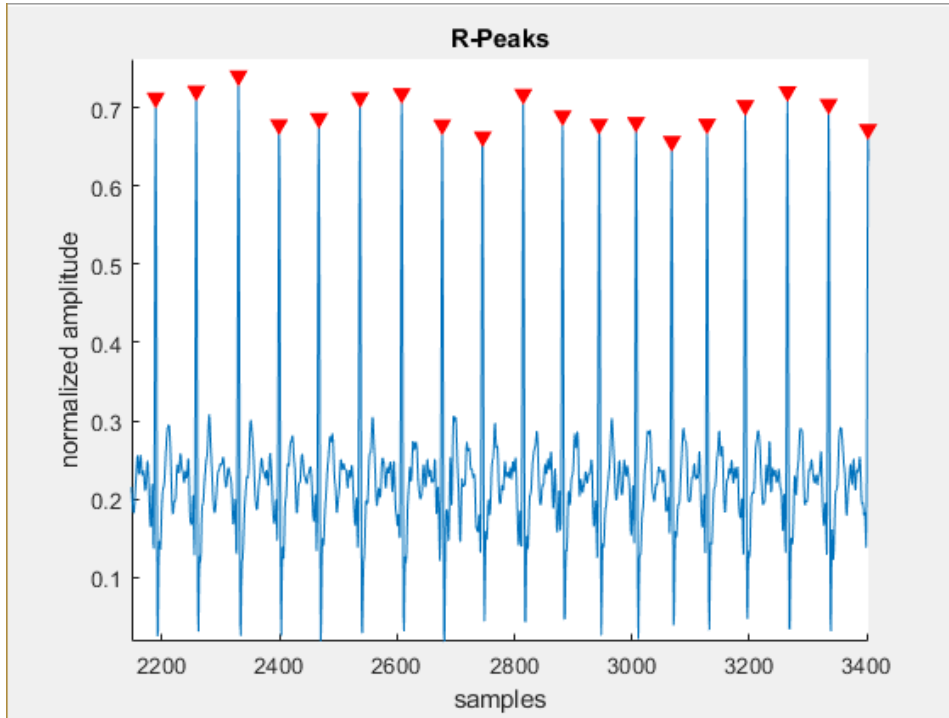


Figure 2.14: Graph of the same ECG signal segment after normalization with amplitudes varying around 0.7mV.

(193bpm) and the lowest (50bpm) heart rate that were accepted. The remaining RR-distances were used to calculate average HR, minimum HR and maximum HR, that were measured during the experiment as well as the baseline. According to 1.5 we proceeded by computing the instantaneous HR for the entirety of the measurement.

In the final step of ECG feature extraction, we determined the HRV by calculating variations in HR between two adjacent data points along the RR-interval vector, using 2.14.

$$HRV = 1./RR_{int} \quad (2.14)$$

Skin Conductance Level

As mentioned earlier, EDA is highly susceptible to environmental influences, such as room temperature and humidity. To be able to estimate a subject's EDR correctly, we therefore included a baseline measurement into our experiment. By subtracting the mean value of the baseline measure we attempted to negate all situational effects on the EDA

measurement. Differences in the tonic level were therefore computed as actual variations in SCL.

Skin Conductance Response

In order to be able to extract the phasic component of the baseline adjusted EDA signal we attempted to filter all tonic components. We therefore applied three different methods, of which two were the inbuilt Matlab functions *detrend*⁶ and *medfilt1*, and self developed moving average filter. When *medfilt1* is used a one-dimensional median filter of order n, that considers the signal to be 0 beyond its endpoints, is applied to the EDA signal. We, on the other hand, have designed an averaging filter that calculates the mean value inside a certain window, of width w, around the current data point, while moving along the signal vector. When close to the endpoints the window size is adapted accordingly and only original values are considered in the calculation. In figure 2.15 the results of each method are shown on a recorded and baseline adjusted EDA measurement.

⁶This function was already described in an earlier section. Therefore it will not be explained at this point.

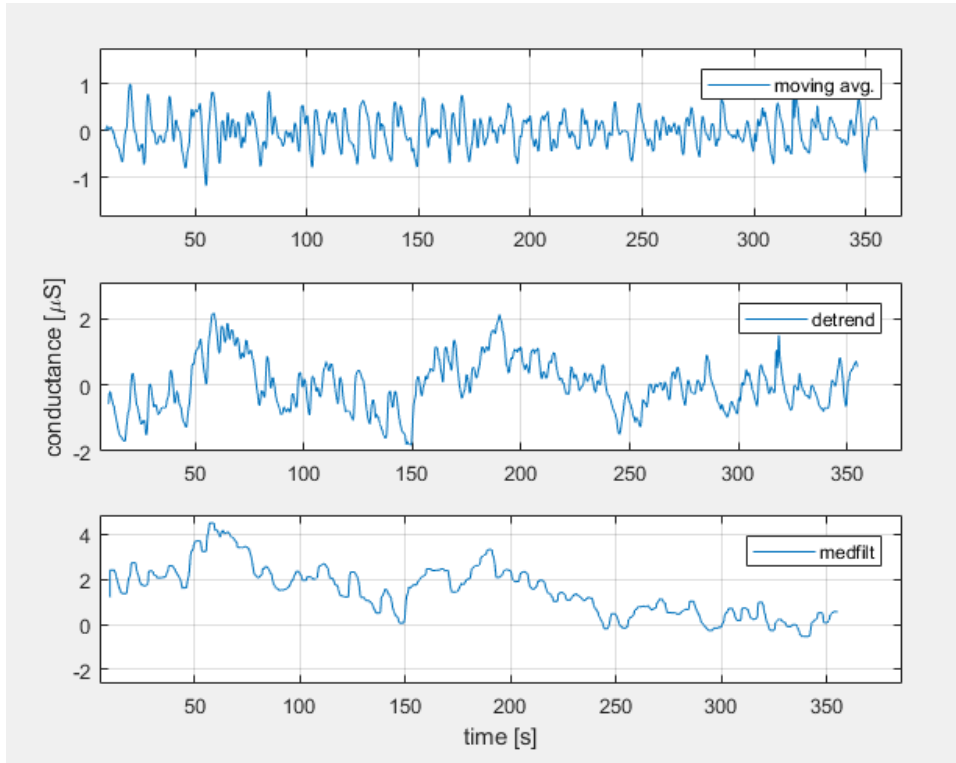


Figure 2.15: Graphical illustration of the results of SCL negation methods. From top to bottom: moving average filter, detrend function and one-dimensional medfilt function.

After the application of our SCL negation method, we located peaks in the EDA signal, using the *findpeaks* function together with a prominence threshold of $0.01 \mu\text{S}$ and proceeded according to section 2.2.6, extracting the peak distances as well as average peaks per second, for both the exposure and the baseline measurements.

Statistical Methods

In this final step of data evaluation we conducted three different statistical tests on the extracted features to evaluate the effect of our experiment on the subjects, including Shapiro-Wilk test, t-test and effect size. Due to our small sample sizes we had to test for normality in our samples before we were able to conduct the latter two. Thus, we conducted the Shapiro-Wilk test, which tests the null hypothesis (H_0) that a certain sample x , containing n values, came from a normally distributed population. The test statistic W was calculated using the equation 2.15, with n being the sample size, $x(i)$ being the i -th in the size sorted sample and \bar{x} being the arithmetic average of the sample x .

$$W = \frac{\left(\sum_{i=1}^n a_i \cdot x(i)\right)^2}{\sum_{i=1}^n (x_i - \bar{x})^2} \quad (2.15)$$

The coefficients a_i as well as $W_{critical}$, were chosen in regard to the sample size n and the significance level α . If W was found to be greater than the associated $W_{critical}$ the null hypothesis H_0 , and therefore normality, could be confirmed [33].

In the next step we conducted a two-sample t-test for paired samples, which is also called a paired difference test. This test is commonly used for a group of units, in our case the subjects, that has been tested twice. In our case we tested the null hypothesis ?? that the mean values of our paired samples would not differ. One pair was comprised of a subject's baseline measurement as well as its exposure measurement. Therefore we calculated the t-value using the equation 2.17, with \bar{X}_D being the mean difference in all pairs and s_D being the standard deviation of the differences.

$$H_0 : \mu_D = 0 \quad (2.16)$$

$$t = \frac{\bar{X}_D - \mu_0}{\frac{s_D}{\sqrt{n}}} \quad (2.17)$$

$$s = \sqrt{\frac{\sum_{i=1}^n (x_i - \bar{x})^2}{n-1}} \quad (2.18)$$

The final evaluation we performed a test on the effect size to determine the power of the two-sample t-test. "The population standardized mean difference was proposed by Cohen (1969) as an index of effect magnitude in connection with an assessment of the power of the two-sample t-test. We denote this population parameter by δ and its unbiased estimate by d " (see [34], p.108). The Cohen's d , for samples of same size but different variances, is defined as the difference between the means of the two samples divided by the pool variance (see 2.19) [35].

$$d = \frac{\bar{x}_1 - \bar{x}_2}{\sqrt{\frac{s_1^2 + s_2^2}{2}}} \quad (2.19)$$

According to Cohen small effects are indicated by a d value of 0.2, medium effects by 0.5 and large effects for d value above or equal to 0.8 .

3 Results

3.1 Electrodermal Activity

We have plotted the average SCL of all subjects during the baseline and exposure measurement in the form of boxplots, as can be seen in figure 3.2. Additionally we included the overall average differences in SCL between the two measurements.

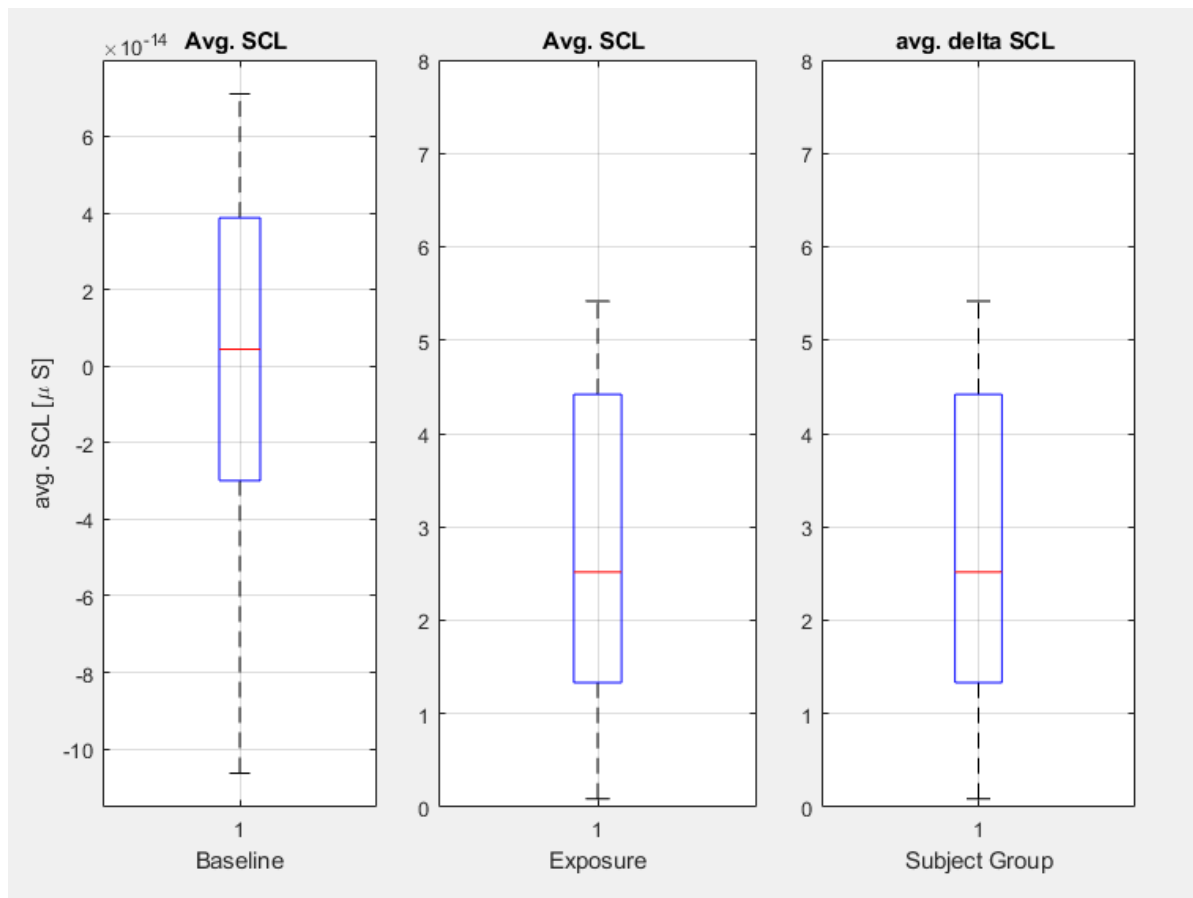


Figure 3.1: Boxplot comparison of the average SCL in subject's baseline (left) and exposure measurement (middle) as well as the average difference in the SCL of the two measurements (right).

In figure 3.2 the peak interval distributions of each subject were illustrated in the form of a boxplot for both the baseline and the exposure measurement. The median RR interval is indicated by a red, horizontal line inside the box. The lower and the upper quartile are displayed by the lower and upper edge of the box, respectively. Minimum and maximum value of the peak interval sample are indicated by the endpoints of the, so called, whiskers (outliers are marked as red +).

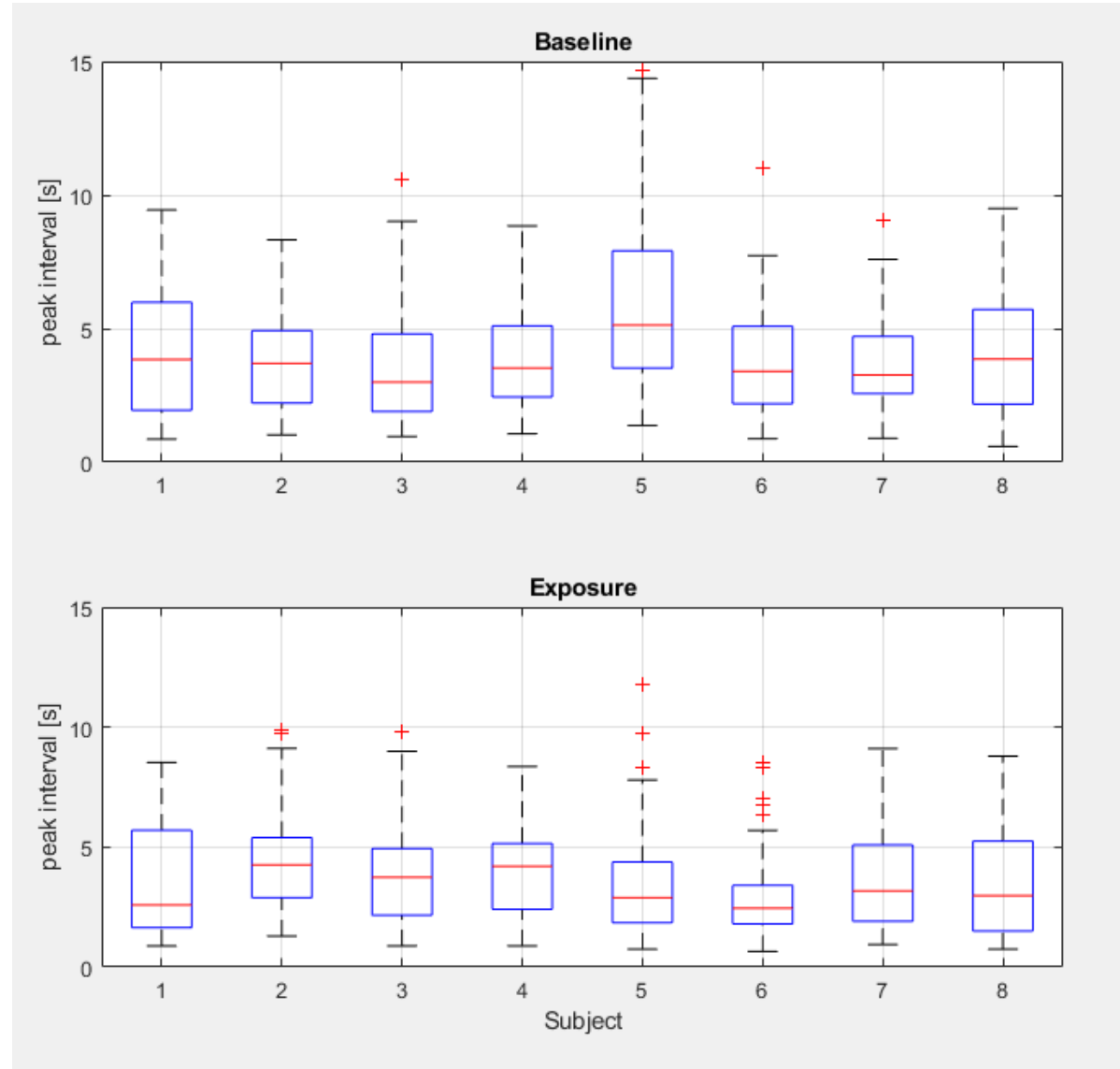


Figure 3.2: Boxplot comparison of the peak interval distribution of subject's baseline and exposure EDA measurement.

An example of an alternative way to illustrate the peak interval distribution is shown in figure 3.2. We have created histograms for each subject indicating the frequency of the measured peak intervals.

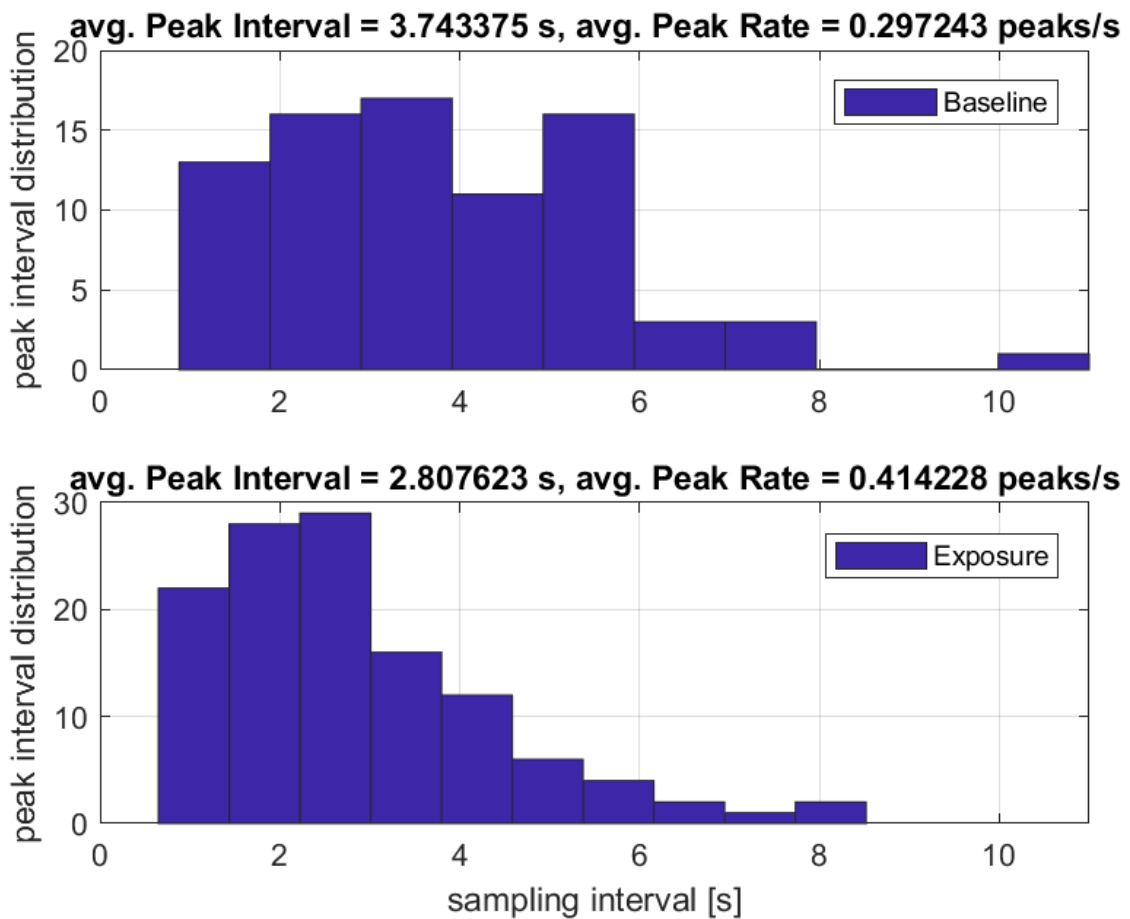


Figure 3.3: Histogram, illustrating the peak interval distribution of a subject's baseline and exposure EDA measurement.

3.2 Electrocardiogram

According to the illustration of EDA, the RR intervals of all subjects are presented in similar fashion in figure 3.4. As well as the individual RR distribution in figure 3.5.

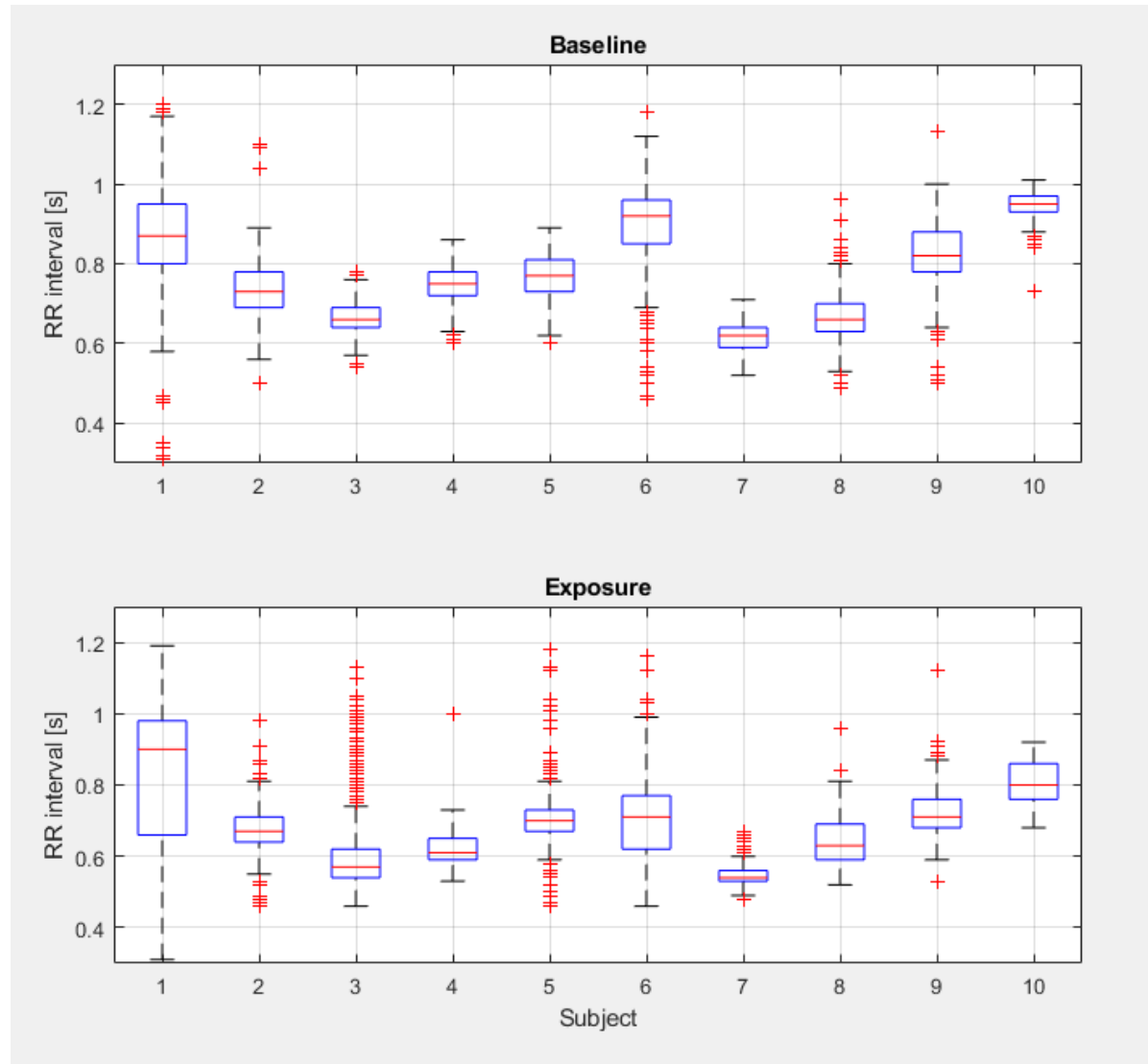


Figure 3.4: Boxplot comparison of the RR interval distribution of subject's baseline and exposure ECG measurement.

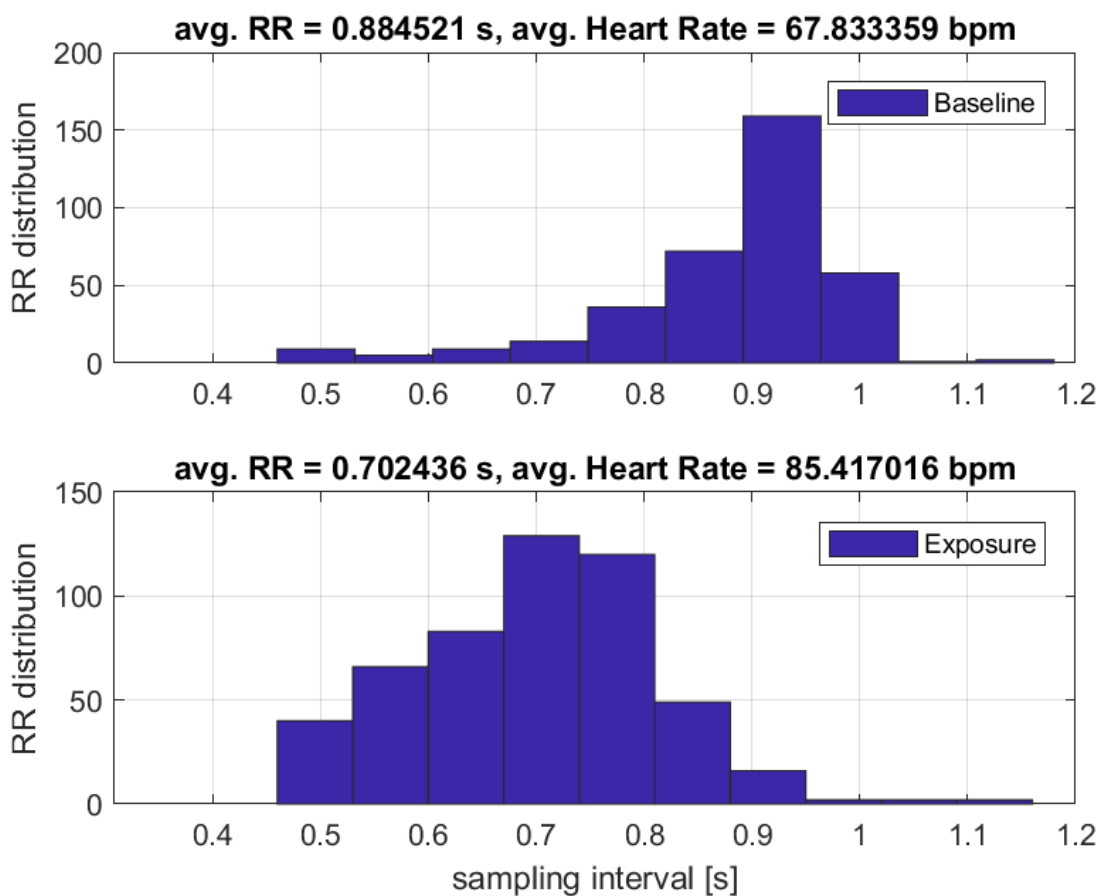


Figure 3.5: Histogram, illustrating the RR interval distribution of a subject's baseline and exposure ECG measurement.

3.3 Statistical Results

Table 3.1: Results: Shapiro Wilk test

sample x	n	α	W	$W_{critical}$	\bar{x}	a_i	H
EDA BL	8	0.05	0.6621	0.818	4.1107	0.6052 0.3164 0.1743 0.0561	1
EDA EP	8	0.05	0.8318	0.818	4.0032	0.6052 0.3164 0.1743 0.0561	0
SCL BL	8	0.05	0.8476	0.818	-1.0882e-15	0.6052 0.3164 0.1743 0.0561	0
SCL EP	8	0.05	0.9511	0.818	3.3930	0.6052 0.3164 0.1743 0.0561	0
ECG BL	10	0.05	0.9596	0.842	0.7720	0.5739 0.3291 0.2141 0.1224 0.0399	0
ECG EP	10	0.05	0.9650	0.842	0.6834	0.5739 0.3291 0.2141 0.1224 0.0399	0

Table 3.2: Results: two-sample t-test

sample x	n	α	df	V_{out}	d	t	H
EDA	8	0.05	7	1.895	0.1074	0.2175	0
SCL	8	0.05	7	1.895	3.3930	2.9112	1
ECG	10	0.05	9	1.833	0.0886	5.8845	1

Table 3.3: Results: effect size test

sample 1	sample 2	n	mean 1	mean 2	σ	d	r
EDA EP	EDA BL	8	4.0032	4.1107	0.9150	0.1174	0.0073
SCL BL	SCL EP	8	-1.0882e-15	3.3930	2.3310	1.4556	0.0906
ECG EP	ECG BL	10	0.6834	0.7720	0.0983	0.9010	0.0450

4 Discussion

5 Conclusions

A Tables and Measurement Results

Electrodermal measures, definitions, and typical values		
Measure	Definition	Typical Values
Skin conductance level (SCL)	Tonic level of electrical conductivity of skin	2–20 μ S
Change in SCL	Gradual changes in SCL measured at two or more points in time	1–3 μ S
Frequency of NS-SCRs	Number of SCR in absence of identifiable eliciting stimulus	1–3 per min
SCR amplitude	Phasic increase in conductance shortly following stimulus onset	0.1–1.0 μ S
SCR latency	Temporal interval between stimulus onset and SCR initiation	1–3 s
SCR rise time	Temporal interval between SCR initiation and SCR peak	1–3 s
SCR half recovery time	Temporal interval between SCR peak and point of 50% recovery of SCR amplitude	2–10 s
SCR habituation (trials to habituation)	Number of stimulus presentations before two or three trials with no response	2–8 stimulus presentations
SCR habituation (slope)	Rate of change of ER-SCR amplitude	0.01–0.5 μ S per trial

Key: SCL, skin conductance level; SCR, skin conductance response; NS-SCR, nonspecific skin conductance response.

Figure A.1: Electrodermal measures, definitions and typical values.

List of Figures

1.1	The Layers of the skin.	12
1.2	A artificial cross-section of the skin, combining a sweat gland in ridged skin (left) and a hair together with a sebaceous gland in polygonal skin (right).	13
1.3	Anatomy of the eccrine sweat gland in various layers of glabrous skin.(Adapted from Hassett, 1978)	14
1.4	Skin afferents and efferents at spinal cord level and connections with ascending and descending pathways. —: motoric pathway, -.-: sympathetic efferents.	15
1.5	Central elicitation of EDA in humans. 1: Ipsilateral influences from the limbic system via hypothalamic thermoregulatory areas; 2: Contralateral influences from premotor cortical and basal ganglia areas; 3: Reticular influences. Dashed: Connections within the limbic system.	17
1.6	Three electrode placements for recording EDA.	20
1.7	Graphical representation of principal EDA components.	21
1.8	Ventral perspective of the systemic and pulmonary circulation. Lighter gray areas indicate oxygenated blood and darker gray areas indicate deoxygenated blood.	24
1.9	A: General morphology of the ECG showing P, Q, R, S, and T components, the PR, ST and QRS intervals, the st segment, and the T wave amplitude; B: The heart, conducting system, and Einthoven's triangle. Open arrows indicate the direction of propagation of electrical activation and the associated component of the ECG.	26
1.10	The graphic shows two full cardiac cycles for various aspects, which can be seen on the right.	27
1.11	Summary of all major components of the ECG graph.	28
2.1	Graphical overview of the BITalino device including all functional blocks.	36
2.2	A side view of the VR room in its default configuration.	39
2.3	A top view of the VR room in its default configuration.	40
2.4	Comparison of the different stages of floor opening.	41
2.5	Illustration of 4 different platform position.	42
2.6	Comparison of the different widths of the bridge.	43
2.7	Photograph of the experimental setup, located in the Green Lab in the University Hospital Saarland in Homburg. View on the control desk.	44

2.8	Photograph of the experimental setup, located in the Green Lab in the University Hospital Saarland in Homburg. View on the exposure area	45
2.9	Closed-loop virtual reality system. The grey line illustrates the closed loop information flow.	46
2.10	Example for electrode placement on a right handed subject.	47
2.11	Raw data of an EDA measurement.	49
2.12	FFT of an EDA raw data set.	50
2.13	Graph of a filtered ECG signal segment with amplitudes varying around 0.6mV.	53
2.14	Graph of the same ECG signal segment after normalization with amplitudes varying around 0.7mV.	54
2.15	Graphical illustration of the results of SCL negation methods. From top to bottom: moving average filter, detrend function and one-dimensional medfilt function.	56
3.1	Boxplot comparison of the average SCL in subject's baseline (left) and exposure measurement (middle) as well as the average difference in the SCL of the two measurements (right).	58
3.2	Boxplot comparison of the peak interval distribution of subject's baseline and exposure EDA measurement.	59
3.3	Histogram, illustrating the peak interval distribution of a subject's baseline and exposure EDA measurement.	60
3.4	Boxplot comparison of the RR interval distribution of subject's baseline and exposure ECG measurement.	61
3.5	Histogram, illustrating the RR interval distribution of a subject's baseline and exposure ECG measurement.	62
A.1	Electrodermal measures, definitions and typical values.	67

List of Tables

3.1	Results: Shapiro Wilk test	63
3.2	Results: two-sample t-test	64
3.3	Results: effect size test	64

Bibliography

- [1] J. Layton. How fear works, 2005. URL <<https://science.howstuffworks.com/life/inside-the-mind/emotions/fear.htm>>.
- [2] G. Fink. *Stress Consequences: Mental, Neuropsychological and Socioeconomic*. Elsevier Science, 2010. ISBN 9780123751751. URL <https://books.google.de/books?id=E20HsuKHxaEC>.
- [3] *Diagnostic and Statistical Manual of Mental Disorders*.
- [4] H.-P. Kapfhammer, D. Huppert, E. Grill, W. Fitz, and T. Brandt. Visual height intolerance and acrophobia: clinical characteristics and comorbidity patterns. *European Archives of Psychiatry and Clinical Neuroscience*, 265(5):375–385, 2015. ISSN 1433-8491. doi: 10.1007/s00406-014-0548-y.
- [5] W.T. O'Donohue and J.E. Fisher. *Cognitive Behavior Therapy: Core Principles for Practice*. Wiley, 2012. ISBN 9781118228876. URL <https://books.google.de/books?id=qawT0W2MJI8C>.
- [6] W. Boucsein. *Electrodermal Activity*. The Springer Series in Behavioral Psychophysiology and Medicine. Springer US, 2013. ISBN 9781475750935. URL <https://books.google.de/books?id=0hXrBwAAQBAJ>.
- [7] J.L. Bolognia, J.L.J.R.P.R. Jean L. Bolognia, J.L. Jorizzo, and R.P. Rapini. *Dermatology*. Elsevier Health Sciences. ISBN 9789997638991. URL <https://books.google.de/books?id=f2IwYiyh3YUC>.
- [8] J.T. Cacioppo, L.G. Tassinary, and G.G Berntson. *Handbook of Psychophysiology*. Cambridge University Press, 2007.
- [9] W. Boucsein. *Electrodermal Activity*. The Springer series in behavioral psychophysiology and medicine. Springer US, 2012. ISBN 9781461411260. URL <https://books.google.de/books?id=6N6rnOEZEEoC>.
- [10] *A Guide for Analysing Electrodermal Activity (EDA) and Skin Conductance Responses (SCRs) for Psychological Experiments*.

- [11] ABM Abdullah. *ECG in Medical Practice*. Jaypee Brothers,Medical Publishers Pvt. Limited, 2014. ISBN 9789351520061. URL <https://books.google.de/books?id=cC2HAWAAQBAJ>.
- [12] A.L. Goldberger, Z.D. Goldberger, and A. Shvilkin. *Clinical Electrocardiography: A Simplified Approach E-Book*. Elsevier Health Sciences, 2017. ISBN 9780323508773. URL <https://books.google.de/books?id=q59tDgAAQBAJ>.
- [13] Electrophysiology Task Force of the European Society of Cardiology the North American Society of Pacing. Heart rate variability. *Circulation*, 1996.
- [14] G.G. Bernston, T.J. Bigger, D.L. Eckberg, P. Grossman, P.G. Kaufmann, M. Malik, H.N. Nagaraja, S.W. Porges, J.P. Saul, P.H. Stone, and M.W. Van Der Molen. Heart rate variability: Origins, methods, and interpretive caveats. *Psychophysiology*, 34(6):623–648, 1997. ISSN 1469-8986. doi: 10.1111/j.1469-8986.1997.tb02140.x. URL <http://dx.doi.org/10.1111/j.1469-8986.1997.tb02140.x>.
- [15] G. Riva. Virtual environments in clinical psychology. *Psychotherapy: Theory, Research, Practice, Training*, 40(1/2):68–76, 2003. doi: <https://doi.org/10.1037/0033-3204.40.1/2.68>.
- [16] R.C. Kessler, P. Berglund, O. Demler, R. Jin, K.R. Merikangas, and E.E. Walters. Lifetime prevalence and age-of-onset distributions of dsm-iv disorders in the national comorbidity survey replication. *Archives of General Psychiatry*, 62(6):593–602, 2005. doi: 10.1001/archpsyc.62.6.593. URL <http://dx.doi.org/10.1001/archpsyc.62.6.593>.
- [17] R. J. DeRubeis and P. Crits-Christoph. Empirically supported individual andgroup psychological treatments for adult mental disorders. *Journal of Consulting and Clinical Psychology*, 66(1):37–52, 1998. doi: <http://dx.doi.org/10.1037/0022-006X.66.1.37>.
- [18] B.O. Rothbaum, L.F. Hodges, R. Kooper, D. Opdyke, J.S. Williford, and M. North. Effectiveness of computer-generated (virtual reality) graded exposure in the treatment of acrophobia. *The American Journal of Psychiatry*, 152(4):626–628, 1995. doi: <https://doi.org/10.1176/ajp.152.4.626>.
- [19] K. Cavanagh and D. A. Shapiro. Computer treatment for common mental health problems. *Journal of Clinical Psychology*, 60(3):239–251, 2004. ISSN 1097-4679. doi: 10.1002/jclp.10261. URL <http://dx.doi.org/10.1002/jclp.10261>.
- [20] A. Garcia-Palacios, C. Botella, H. Hoffman, and S. Fabregat. Comparing acceptance and refusal rates of virtual reality exposure vs. in vivo exposure by patients with

specific phobias. *CyberPsychology and Behavior*, 10(5):722–724, 2007. doi: <https://doi.org/10.1089/cpb.2007.9962>.

- [21] D. Huppert, E. Grill, and T. Brandt. Down on heights? one in three has visual height intolerance. *Journal of Neurology*, 260(2):597–604, Feb 2013. ISSN 1432-1459. doi: 10.1007/s00415-012-6685-1. URL <https://doi.org/10.1007/s00415-012-6685-1>.
- [22] B. O. Rothbaum, L.F Hodges, S. Smith, J. H. Lee, and L. Price. A controlled study of virtual reality exposure therapy for the fear of flying. *Journal of Consulting and Clinical Psychology*, 68(6):1020–1026, 2000. doi: <http://dx.doi.org/10.1037/0022-006X.68.6.1020>.
- [23] B. O. Rothbaum, L.F Hodges, D. Ready, K. Graap, and R. D. Alarcon. Virtual reality exposure therapy for vietnam veterans with posttraumatic stress disorder. *J Clin Psychiatry*, 62(8):617–622, 2001.
- [24] K. Meyerbröker, N. Morina, G. Kerkhof, and P.M. Emmelkamp. Virtual reality exposure treatment of agoraphobia: a comparison of computer automatic virtual environment and head-mounted display. *Stud Health Technol Inform*, 167:51–56, 2011.
- [25] F. Levy, P. Leboucher, G. Rautureau, and R. Jouvent. E-virtual reality exposure therapy in acrophobia: A pilot study. *Journal of Telemedicine and Telecare*, 2016.
- [26] M.R. Nesse, G.C. Curtis, B.A. Thyer, D.S. McCann, M.J. Hubert-Smith, and R.F. Knopf. Endocrine and cardiovascular responses during phobic anxiety. *Psychosomatic Medicine*, 1985.
- [27] G. W. Alpers and R. Sell. And yet they correlate: Psychophysiological activation predicts self-report outcomes of exposure therapy in claustrophobia. *Journal of Anxiety Disorders*, 22:1101–1109, 2008.
- [28] J. Diemer, N. Lohkamp, A. Mühlberger, and P. Zwanzger. Fear and physiological arousal during a virtual heightchallenge—effects in patients with acrophobia and healthy controls. *Journal of Anxiety Disorders*, 37:30–39, 2016. doi: <http://dx.doi.org/10.1016/j.janxdis.2015.10.007>.
- [29] P.M.G. Emmelkamp, M. Bruynzeel, L. Drost, and C.A.P.G. Van Der Mast. Virtual reality treatment in acrophobia: A comparison with exposure in vivo. *CyberPsychology and Behavior*, 2001.
- [30] J. Pan and W.J. Tompkins. A real-time qrs detection algorithm. *IEEE Transactions On Biomedical Engineering*, 1985.

- [31] L. Tan and J. Jiang. *Digital Signal Processing: Fundamentals and Applications*. Elsevier Science, 2013. ISBN 9780124159822. URL <https://books.google.de/books?id=M9-0haJSwAEC>.
- [32] The Mathworks Inc. Matlab documentation, 1994-2017. URL <https://de.mathworks.com/help/matlab/index.html>.
- [33] S.S. Shapiro and M.B. Wilk. An analysis of variance test for normality (complete samples). *Biometrika*, 52(3-4):591–611, 1965. doi: 10.1093/biomet/52.3-4.591. URL <http://dx.doi.org/10.1093/biomet/52.3-4.591>.
- [34] L.V. Hedges and I. Olkin. *Statistical Methods for Meta-Analysis*. Elsevier Science, 2014. ISBN 9780080570655. URL <https://books.google.de/books?id=7GviBQAAQBAJ>.
- [35] F.J. Gravetter, L.B. Wallnau, and L.A.B. Forzano. *Essentials of Statistics for The Behavioral Sciences*. Cengage Learning, 2016. ISBN 9781337098120. URL <https://books.google.de/books?id=LNq5DQAAQBAJ>.